Journal of the Korean Ceramic Society
Vol. 55, No. 3, pp. 185~202, 2018.

https://doi.org/10.4191/kcers.2018.55.3.08

Review

Solution-Processed Metal Oxide Thin Film Nanostructures for Water Splitting Photoelectrodes: A Review

Mi Gyoung Lee†, Jong Seong Park†, and Ho Won Jang‡

Department of Materials Science and Engineering, Research Institute of Advanced Materials, Seoul National University, Seoul 08826, Korea

(Received February 28, 2018; Revised March 22, 2018; Accepted March 26, 2018)

ABSTRACT

Photoelectrochemical (PEC) cells can convert solar energy, the largest potential source of renewable energy, into hydrogen fuel which can be stored, transported, and used on demand. In terms of cost competitiveness compared with fossil fuels, however, both photocatalytic efficiency and cost-effectiveness must be achieved simultaneously. Improvement of cost-effective, scalable, versatile, and eco-friendly fabrication methods has emerged as an urgent mission for PEC cells, and solution-based fabrication methods could be capable of meeting these demands. Herein, we review recent challenges for various nanostructured oxide photoelectrodes fabricated by solution-based processes. Hematite, tungsten oxide, bismuth vanadate, titanium oxide, and copper oxides are the main oxides focused on, and various strategies have been attempted with respect to these photocatalyst materials. The effects of nanostructuring, heterojunctions, and co-catalyst loading on the surface are discussed. Our review introduces notable solution-based processes for water splitting photoelectrodes and gives an outlook on eco-friendly and cost-effective approaches to solar fuel generation and innovative artificial photosynthesis technologies.

Key words : Metal oxides, Solution process, Electrodeposition, Hydrothermal, Photoelectrochemical water splitting

1. Introduction

1.1. Needs for Photoelectrochemical Water Splitting

The depletion of conventional fossil fuels, which are insufficient to meet the energy requirements of an increasing population, is of growing concern for the human race and for socially sustainable development.[1-6] Thus it is extremely urgent to search for viable alternative renewable energy sources to replace fossil fuels. Renewable energy sources include solar, wind, wave, and biomass, among which solar energy possesses a theoretical potential of 1.2×10^5 TW, more than any other energy source,[2] and could in theory easily meet the world's total energy consumption. Solar electricity produced by photovoltaics is still very expensive, difficult to store for long periods, and challenging to distribute over long distances; hence, the efficient and inexpensive conversion of solar energy into chemical energy such as hydrogen is considered a highly desirable way to satisfy long-term energy needs and cost-effectiveness, as shown in Fig. 1(a) and Table 1.[7-8] Among envisioned approaches, as shown in Fig. 1(b), photoelectrochemical (PEC) water splitting has attracted considerable interest for storing solar energy in chemical bonds via generation of hydrogen.[3,8-13]

The unit costs of various energy sources, stated in Table 1,[7] demonstrate that lowering the energy production cost of PEC water splitting should be treated as an urgent mission for satisfying its cost competitiveness compared with fossil fuel.[14] The United States Department of Energy (US-DOE) stated in 2011 that the upper limit cost of hydrogen in 2020, which would make this a feasible fuel, would be 2 - 4 USD per kg.[7] The present cost target for hydrogen generation with PEC water splitting, 5.7 USD per kg, must be further reduced to meet the maximum cost suggested by US-DOE. A similar proposal was announced by the Ministry of Economy, Trade and Industry (METI) of Japan in 2008. METI suggested 40 JPY per Nm^3, which is of similar value to the US-DOE proposal, as a hydrogen cost target in 2020.[7] Table 1,[7] put together by Sayama in 2015, shows the unit energy costs of various energy resources including current energy resources and renewable sources with high potential. It can be seen that the unit energy cost of current energy resources are usually below 2 JPY per MJ, and the unit energy costs of renewable energy sources are much more expensive than current energy resources. Even though the cost for fossil fuel seems to be on the rise, a further reduction in renewable energy costs is imperative. This is especially true in the case of hydrogen production by PEC water splitting; according to the analysis of Shaner,[15] simply attaining very high solar-to-hydrogen conversion efficiency will not guarantee PEC water splitting technology becoming a cost-competitive energy resource. In this regard, much greater advances in system cost reduction are needed.

†These authors contributed equally to this work.
‡Corresponding author : Ho Won Jang
E-mail : hwjang@snu.ac.kr
Tel : +82-2-880-1720 Fax : +82-2-865-9671

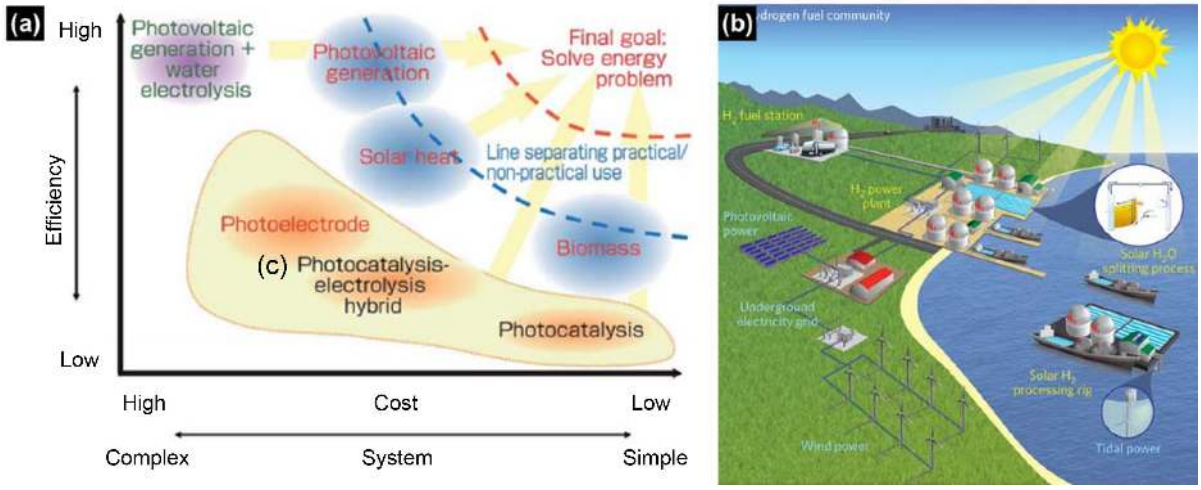

Fig. 1. (a) Technological map showing various approaches to solar energy conversion. Adapted with permission from Ref 7. (b) Vision of a sustainable hydrogen fuel community based photoelectrochemical water splitting. Adapted with permission from Ref 16.

Table 1. Comparison of Unit Energy Cost. Adapted with Permission from Ref 7

Energy	Cost/JPY per MJ	Remark
Gasoline	1.8 - 2.6	In 2010
Petroleum	1.4 - 1.8	In 2010
Liquid natural gas	0.7 - 1.7	In 2010
Coal	< 0.3	In 2010
Fossil fuel (average)	1.0 - 1.5	In 2010
Hydrogen	2.4	Target in 2020
PV	6.4 - 10.6	In 2013
PV	1.9	Target in 2030
PV + water-electrolysis	10.9	In 2014
Wind Power	2.6 - 6.4	In 2010, estimated to be similar in 2030
Biomass-fired power	4.8 - 8.9	In 2010
Biomass-ethanol	1.7 - 4.3	Target

Figure 1(b), suggested by Tachibana *et al.* in 2012,[16] demonstrates a design for an artificial photosynthesis plant using available renewable energy such as tide, wind, and solar energy for maintenance cost reduction. It would be possible to implement this kind of facility in any seashore or off-shore location where seawater could be pumped and filtered efficiently. However, in order to fulfill large amounts of energy demand with hydrogen fuels, the implementation of large area PEC cells would also be needed. As stated by Maeda *et al.*,[17] a solar hydrogen plant with PEC cells (solar energy conversion efficiency of 10%) having an area of 25 km^2 would produce 570 tons of hydrogen from 5100 tons of water per day. And to supply one-third of the world's energy requirements in 2050, tens of thousands of hydrogen plants would be needed. To satisfy these demands, scalable, and cost-effective fabrication systems for PEC cells would need to be developed and well-established.[18]

1.2. Advantages of Solution Process

From this point of view, solution fabrication methods, such as hydrothermal and electrophoretic deposition, are attractive in terms of their scalability, financial advantages and eco-friendliness.[14,19-24] As displayed in Fig. 2, vacuum processes that are currently widely used for many film fabrication methods aggravate global environmental load. Additionally, not only low-pressure fabrication methods but also high-pressure and high-temperature methods contribute environmental load. Without escaping from these types of fabrication method, it is impossible to avoid worsening the environmental footprint. One of the biggest reasons for replacing fossil fuel with renewable energies is to minimize the additional environmental footprint, which makes the advancement of cost-effective and eco-friendly fabrication methods for PEC cells an urgent challenge. Overall, it is obvious that solution based-fabrication methods are a very promising pathway for PEC cell fabrication.

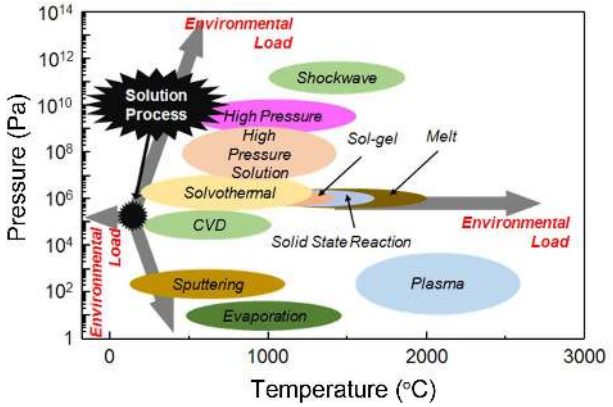

Fig. 2. Needs to proceed to solution processes in the future. The schematic shows energy efficiency improvement of solution processes.

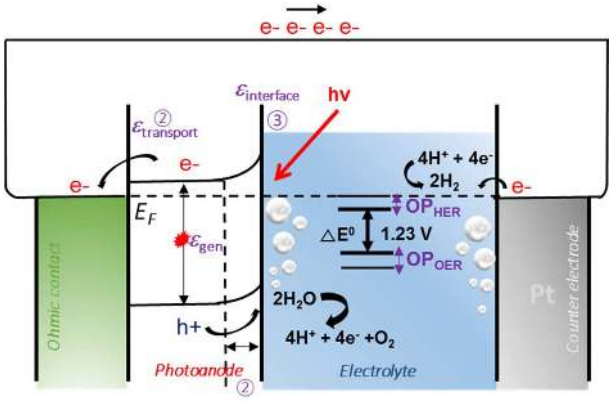

Fig. 3. Principle and critical parameters of photoelectrochemical solar water splitting system. Schematic is described in terms of the photoanode as an n-type semiconductor.

1.3. Basic Principles of Photoelectrochemical Water Splitting

The fundamental principle and critical factors of PEC water splitting are displayed in Fig. 3. The interaction of light with a semiconductor as the photoanode generates electron and hole pairs in the semiconductor. The electrons can be excited from the valence band (VB) to the conduction band (CB) of the semiconductor under irradiation by light of suitable wavelengths, leaving holes in the VB.[1-2,8,16,25] These electrons and holes can then transfer to the surface of the photoelectrode and initiate hydrogen and oxygen evolution reaction (HER and OER), respectively. Thus, the position of the CB and VB energy levels of the photoelectrode is crucial to achieve efficient solar water splitting. From a thermodynamic point of view, the minimum of the CB must be located at a more negative potential than the reduction potential of H^+ to H_2 (0.41 V vs. NHE at pH 7), while the maximum of the VB must exceed the oxidation potential of H_2O to O_2 (0.82 V vs. NHE).[1] In order to drive the water splitting reaction, the photoelectrode must absorb light irradiation to make its electrode potential higher than 1.23 V. In addition, due to energy losses, a kinetic overpotential (OP) is needed to drive the HER and the OER, and thus the band gap energy (E_g) of the semiconductors as photoelectrodes should lie in the range of 1.5 to 3.1 eV, which is within the visible range of the solar spectrum.[2] The key criteria for efficient solar water splitting are expressed as the product or the light absorption efficiency; the charge separation efficiency and the injection efficiency of the photogenerated carriers to the reactants; a broad light absorption range; efficient charge transfer from the bulk of the semiconductor to the surface; and rapid consumption of the photogenerated carriers for the surface reaction with minimum overpotential.[2,8,26]

Another critical factor, which may limit the utilization of several photoelectrode materials, is resistance to photocorrosion, or electrochemical stability. Many non-oxide semiconductors show poor stability due to undesired photocorrosion or anodic photodecomposition, while metal oxide semiconductors are usually more stable over a wide range of

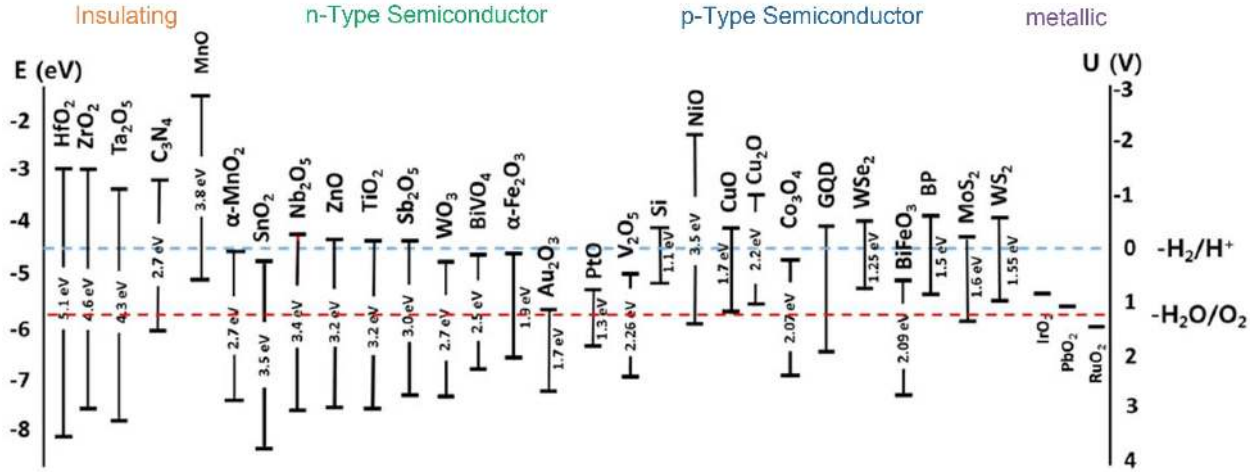

Fig. 4. Band gap energies and band alignments for various PEC water splitting materials.

pH values in aqueous environments upon illumination. Metal oxides attract considerable attention due to their excellent chemical stability, suitable band edge positions, low cost, and tunable bandgaps.[1,8,11,27] Metal oxides are usually one of the most stable forms of metal compounds in nature and can be easily synthesized.[8,28] Moreover, metal oxides have a wide distribution of band gap and band edge positions, as shown in Fig. 4.

To design highly efficient photoelectrodes for water splitting, all of these typical processes such as light absorption, charge separation, transport, and utilization must be comprehensively considered and optimized. The current bottleneck of photoelectrodes is a lower quantum yield than theoretical values, which is strongly affected by severe electron-hole recombination, sluggish photo-generated carrier transport and extraction, surface back reaction, and poor stability.[3,26] So far, the efficiency improvement of photoelectrodes is one of the most challenging tasks in solar water splitting systems for practical use. A variety of strategies such as nanostructuring, heterojunction, and co-catalysts have been developed to address the aforementioned drawbacks of metal oxide photoelectrodes for PEC water splitting, and these are summarized in Fig. 5.[29] Most of all, compared to their bulk counterparts, nanostructured materials with smaller size and larger interfacial surface area can effectively shorten the diffusion distance for photo-excited charge carriers and facilitate electron-hole separation at the electrode/electrolyte interface, thus improving charge collection and utilization efficiency.[3,10,16] Therefore, in this review, we focus primarily on nanostructured photoelectrodes with outstanding photoactivity.

This review covers the fundamental aspects of PEC water splitting, focusing primarily on nanostructured metal oxide semiconductors synthesized by solution processes. We report on several studies using nanostructured metal oxides as photoelectrodes for PEC water splitting. The limitations

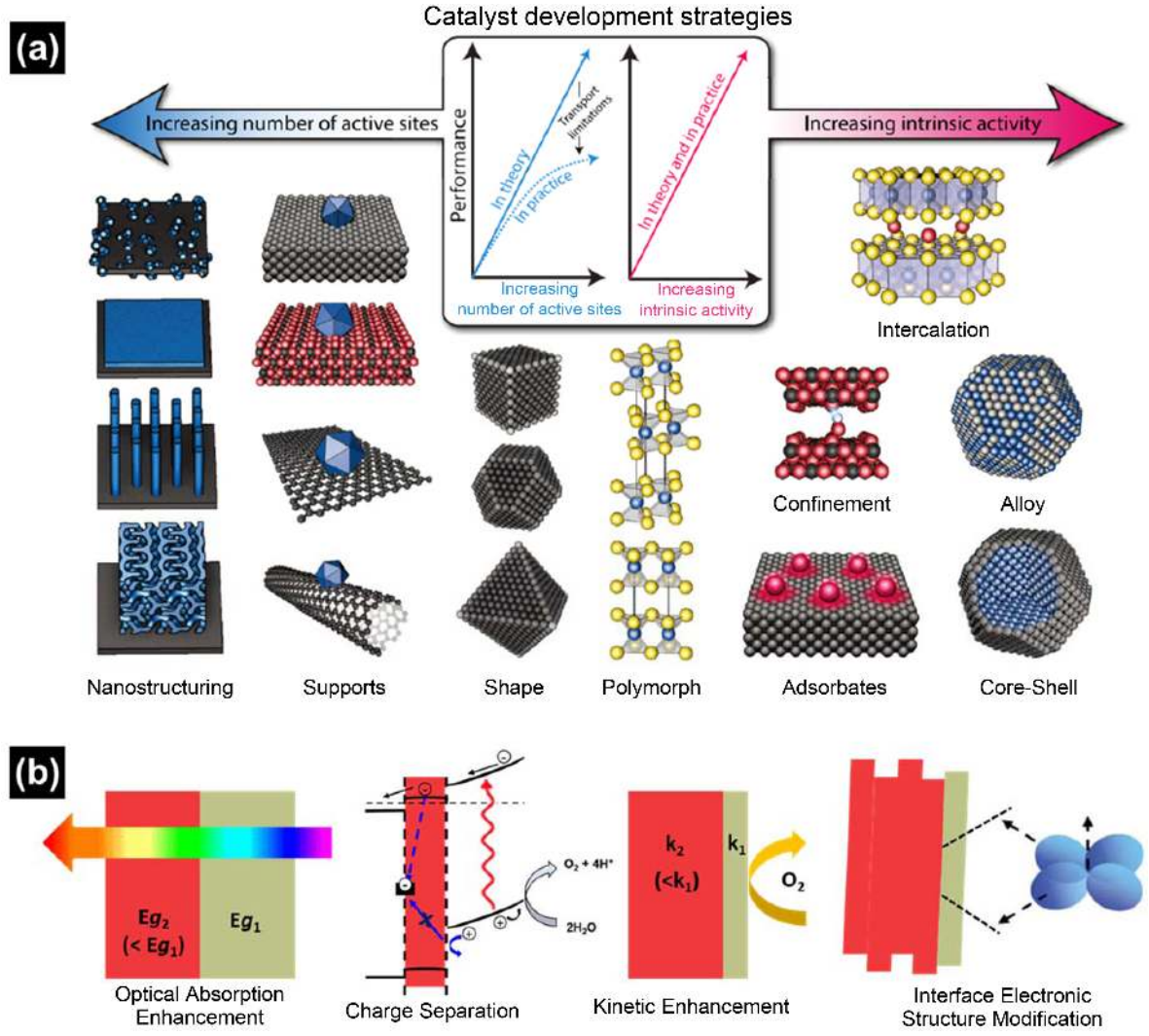

Fig. 5. Catalyst development strategies for efficient solar water splitting system. (a) Schematic of various catalyst development strategies, which aim to increase the number of active sites and/or increase the intrinsic activity of each active site. Adapted with permission from Ref 29. (b) PEC property enhancements in heterogeneous semiconductor photoelectrode.

of commonly used metal oxide photoanodes and photocathodes for PEC water splitting, as well as the strategies developed to address them, will be thoroughly discussed. Finally, we will provide a brief outlook of the current concepts and future opportunities for metal oxide photoelectrodes in PEC water splitting.

2. Recent Advances in Solution-based Process for Metal Oxide Photoelectrodes

Metal oxides, including Fe_2O_3, $BiVO_4$, WO_3, TiO_2, and Cu_2O, have been extensively explored for PEC water splitting, since they are usually inexpensive, stable, and easily prepared on a large scale for practical applications. To improve the efficiency of metal oxides as photoelectrodes, elemental doping, pairing with various oxygen evolution catalysts (OECs), heterojunctions, and nanostructuring have been studied. Among these, we will focus primarily on diverse nanostructures of metal oxides for water splitting synthesized by solution processes. Table 2 summarizes recent studies of metal oxide photoelectrodes synthesized by solution processes.

Table 2. Recent Reports on Metal Oxide Based Photoelectrodes Synthesized by Solution Process for Solar Water Oxidation

Year	Photoelectrodes	Electrolyte	Performance	Method	Reference
2018	WO_3-NRs/$BiVO_4$+CoPi	0.5 M Na_2SO_4	5.0 mA/cm^2 (1.23 V vs. RHE)	Hydro-depositing/drop casting	53
2017	$LaFeO_3$	0.1 M NaOH (pH 13)	− 0.1 mA/cm^2 (0.73 V vs RHE)	Electrodeposition	103
2017	Au NPs/$BiVO_4$	0.5 M KPi/1 M Na_2SO_3	2.4 mA/cm^2 (1.23 V vs. RHE)	Electrodeposition /dipping	5
2017	CuO	0.1 M KOH (pH 13)	− 3.5 mA/cm^2 (0.6 V vs RHE)	Electrodeposition	100
2016	$BiVO_4$/WO_3 NRs	0.5 M KPi/1 M Na_2SO_3 (pH 7.2)	4.55 mA/cm^2 (1.23 V vs. RHE)	GLAD/Pulsed electrodeposition	3
2016	FeOOH/Fe_2O_3	1 M NaOH (pH 13.6)	1.21 mA/cm^2 (1.23 V vs. RHE)	Solution-based method	47
2016	Pt/TiO_2 NRs/p-Si	0.5 M H_2SO_4	40 mA/cm^2 (0 V vs. RHE)	Hydrothermal/ e-beam evaporation	88
2016	NiFe-LDH/Cu_2O	0.5 M Na_2SO_4 (pH 6.0)	2.42 mA/cm^2 (– 0.6 V vs. Ag/AgCl)	Electrodeposition	94
2016	Cu_2O/CuO	0.5 M Na_2SO_4 (pH 6.0)	− 2.47 mA/cm^2 (0 V vs RHE)	r-DPPC deposition	95
2015	Co-Pi/$BiVO_4$/WO_3-NRs/ITO/Pt/ITO	0.5 M KPi/1 M Na_2SO_3 (pH 7.2)	6.72 mA/cm^2 (1.23 V vs. RHE)	Multi-magnetron GLAD/ electrodeposition	54
2014	Fe-NiOOH/$BiVO_4$	0.5 M KPi/1 M Na_2SO_3 (pH 7.2)	4.16 mA/cm^2 (0.6 V vs. RHE)	Electrodeposition /photo electrodeposition	48
2014	CuO	0.5 M Na_2SO_4 (pH 6.0)	~ 1.2 mA/cm^2 (– 0.55 V vs. Ag/AgCl)	Electrodeposition	98
2013	Au/TiO_2 NRs	1 M KOH (pH 13.6)	2.32 mA/cm^2 (1.23 V vs. RHE)	Hydrothermal/ photoreduction	93
2013	Co-Pi/Pt:Fe_2O_3	1 M NaOH (pH 13.6)	4.32 mA/cm^2 (1.23 V vs. RHE)	Solution-based method	104
2012	$BiVO_4$	0.1 M KPi (pH 7.0)	1.17 mA/cm^2 (0.55 V vs. RHE)	Electrodeposition	51
2012	FeOOH/$BiVO_4$	0.1 M KPi/0.1 M Na_2SO_3 (pH 7.0)	1.7 mA/cm^2 (1.2 V vs. RHE)	Electrodeposition /photo electrodeposition	52
2012	$CuFeO_2$	1 M NaOH (pH 13.6)	0.085 mA/cm^2 (0.6 V vs RHE)	Electrodeposition	101
2012	$CuBi_2O_4$	N_2 degassed Na_2SO_4 (pH 10.8)	33 μA/cm^2 (0.8 V vs. RHE)	Electrodeposition	102
2012	Ni-doped Fe_2O_3	1 M KOH (pH 13.6)	3.3 mA/cm^2 (0.45 V vs. Ag/AgCl)	Electrodeposition	105
2011	TiO_2 nanocrystal	1 : 1 water-methanol solution	13 days stability	Hydrothermal	62
2011	TiO_2	1 M KOH (pH 13.6)	0.83 mA/cm^2 (0.8 V vs. RHE)	Hydrothermal	92

2.1. Photoanodes

2.1.1. Hematite (Fe_2O_3)

Iron is the fourth most common element in the earth, where it is already oxidized into ferrous (+2) or ferric (+3) states. Among the crystal structures of iron oxide, hematite is the most thermodynamically stable form, i.e. the most commonly founded in nature. In consideration of system costs, the cost of materials for photoelectrodes needs to be treated as a serious requirement. Its electronic properties as an n-type semi-conductor make hematite a potentially promising photoanode material. The energy band gap of hematite is usually reported to be in the range of 1.9 to 2.2 eV, corresponding to 650 to 560 nm of wavelength.[30] The absorption of yellow to UV photons that are most abundantly contained in incident photons[31] is strong for this reason. Coupled with its earth-abundance, non-toxicity, and stability in aqueous solution, its electronic properties as a semiconductor make hematite an attractive material for artificial photosynthesis. Exploration of hematite as a solar energy conversion material was first carried out by Hardee and Bard in 1976.[32] They fabricated hematite thin films on Ti and Pt substrates by chemical vapor deposition. Since that time, continuing studies on hematite have been carried out with various fabrication methods, including solution-based processes.[30,33] Herein, only a few notable trials with nanostructured thin films based on solution fabrication methods will be introduced.

Researchers have tried to generate thin films of hematite with donor doping,[34-37] as hematite has a short diffusion length (L_D = 2-4 nm)[37-38] and poor majority carrier conductivity.[35,39] An increase of doping concentration in turn reduces the width of a space-charge layer between the photoelectrode and the electrolyte. When assuming classical depletion layer theory,[40] only 7 nm width of depletion layer is generated in the case of Nb- doped single crystal hematite with a concentration of 5×10^{19} cm^{-3}.[35] However, although dopants were added, the relatively low adsorption coefficient for hematite[41,42] straddles carrier separation if hematite has a planar structure. Because the adsorption depth for planar hematite is in the range of 120 - 46 nm for photon wavelengths of 550 - 450 nm,[43] fast recombination of excitons will be promoted in the case of a simple planar thin film. Consequently, overcoming these limitations has always been treated as the major barrier for hematite utilization.

In this regard, a recently reported study suggests adaptation of doping and nanostructuring simultaneously. Sivula *et al.*[44] reported mesoporous hematite thin films on fluorine-doped tin oxide (FTO) substrate prepared by a solution-based colloidal method. For preparation of the precursor paste, a solution was synthesized by combining 400 mg of Fe_2O_3 nanopowder, with 40 µL of a 10% solution of acetylacetone (Acac) and 1-hexanol using a mortar and pestle. The prepared solution was diluted with 1% Acac in 2-propanol, and this was well-dispersed in a water-bath (10°C) by an ultrasonic tip sonicator. Finally, the dispersed solution was concentrated by evaporation and mixed with a 4 wt% solution of hydroxypropyl cellulose (HPC) in 2-propanol. The prepared precursor paste was coated on FTO substrate by doctor-blade at a thickness of 40 µm, and then annealed by a two-step process in order to remove the organics. Prior to reaching the set point (700 - 800°C), an initial heat treatment was carried out at 400°C for 10 h. Fig. 6(a), (b) shows different particle sizes of hematite with respect to the heat treatment temperature. Even though a specimen prepared at 800°C has larger particle size than at 700°C, a much higher photocurrent density was exhibited by the 800°C specimen. Analysis by XPS (X-ray photoelectron spectroscopy) and UV-Visabsorption spectroscopy showed that doping of Sn from the FTO substrate occurs, due to the high thermal energy which induces large effects on optical properties and photoactivity. Souza *et al.*[45] also tested the effect of doping and nanostructure simultaneously by fabricating nanostructured hematite thin films using a polymeric precursor spin coating method. Both nanostructure and silicon doping concentration were controlled by the concentration of tetraethyl orthosilicate (TEOS), which has the role of sili-

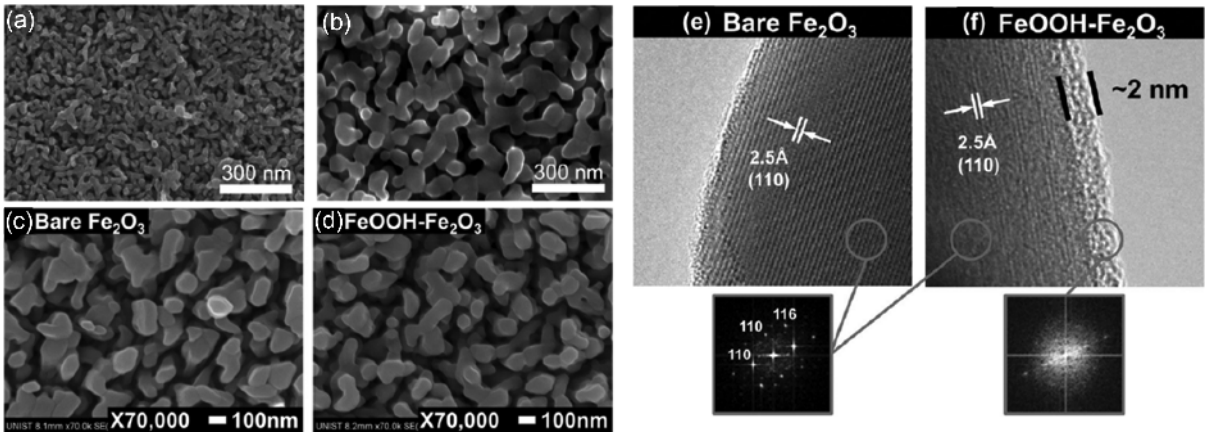

Fig. 6. SEM images of mesoporous hematite fabricated on FTO substrates after annealing: at (a) 700°C and (b) 800°C for 20 min. Adapted with permission from Ref 44. SEM images and HRTEM images for (c) and (e) bare hematite and (d) and (f) hematite covered with amorphous FeOOH layer with a thickness of about 2 nm. Adapted with permission from Ref 47.

con precursor. For the polymeric precursor, iron(III) nitrate 9-hydrate and TEOS dissolved in isopropyl alcohol were stirred in citric acid dissolved in DI water and heated in the range of 70 - 90°C. Promotion of citrate polymerization was done by stirring and heating after adding ethylene glycol to this solution. Although an optimally-controlled doping concentration of Si exhibited enhanced photocurrent density, it could be seen that the effect of Si doping shows much lower impact compared with Sn doping. For this reason, the effect of doping in hematite relies on the proper type of dopant and enough thermal energy. However, enough thermal energy promotes further growth of crystal size, which highlights the short diffusion length of hematite.

Brillet *et al.*[46] conquered this phenomenon by encapsulation with silica, whose role is to confine further growth of the hematite crystals. The experimental procedure for preparation of precursor paste was very similar to Sivula *et al.*,[45] but titanium isopropoxide was also added for Ti ion doping when the solution was mixed with HPC. First, heat treatment was applied, to remove organic compounds. The encapsulation was then performed by chemical bath deposition. The annealed mesoporous hematite thin films were immersed at 0°C in aqueous methanol solution, hexadecyltrimethylammonium chloride, and aqueous ammonia in sequence. The encapsulated hematite films were then annealed at 800°C in air. After heat treatment, the silica layer was etched by dilute aqueous NaOH (5 M). Brillet *et al.* demonstrated an adequate fabrication method to restrict further growth of particle size and an enhancement of the doping effect at high temperature.[46]

Deposition of an FeOOH (oxygen evolution co-catalyst) overlayer on hematite was recently tested by Kim *et al.* for further enhancement of the PEC performance.[47] Mesoporous hematite thin films were prepared by simply immersing a FTO substrate in a solution containing 0.15 M $FeCl_3 \cdot 6H_2O$ and placing it in an oven at 100°C for 6 h. Fig. 6(f) shows the finely coated FeOOH layer. Prepared thin films were annealed via a two-step heat treatment: 550°C for 1 h followed by 20 min annealing at 800°C. The FeOOH overlayer was deposited by simply immersing hematite thin films into an aqueous solution containing 0.15 M $FeCl_3 \cdot 6H_2O$ and 1 M $NaNO_3$ at 100°C for 5 min. An increase in surface reaction can be captured by a decrease of onset potential and a doubling of photocurrent density.

2.1.2. Bismuth Vanadate ($BiVO_4$)

Among oxide photoelectrode candidates, $BiVO_4$ has been identified as one of the most promising n-type semiconductor photoanodes for use in solar water oxidation, since it can absorb a substantial portion of the visible spectrum due to its relatively narrow band gap energy (~ 2.4 eV), and it has a favorable portion of the conduction band very near the thermodynamic hydrogen evolution potential.[3,5,8-9,48] However, inefficient charge transport and interfacial charge transfer properties are the key limiting factors for $BiVO_4$ photoanodes.[3-4,8,48] The presence of a porous nanostructure in the photoelectrodes provides an increased interfacial area between the electrolyte and the film. The formation of nanostructures enables improvement of the water-splitting efficiency, as the photogenerated holes will have to traverse less bulk material to be collected at the solution interface; therefore it has a lower chance of recombining before participating in the electrochemical reaction.[4,27,49] However, increasing the surface area by introducing porosity can also have adverse effects on charge separation and transport, as it can result in an increase in surface states, defect sites, and grain boundaries while decreasing crystallinity. Therefore, the morphologies and surface areas of a photoelectrode should be finely optimized to maximize the overall net positive effect.[27]

One interesting study by Xi *et al.*[50] reports that $BiVO_4$ nanoplates synthesized by a hydrothermal method have monoclinic scheelite structures with well-defined facets exposed at the surface. They compared photoactivities of $BiVO_4$ with different morphologies such as nanorods and nanoplates. The $BiVO_4$ nanoplates showed higher photocurrent density than nanorods due to active surface structures of the $BiVO_4$ nanoplates. This study indicates that designing nanostructures with appropriate surface facets is a feasible approach for the improvement of photoactivity.

$BiVO_4$ has also been prepared by a new cathodic electrodeposition method, as demonstrated by McDonald, Choi *et al.*[51-52] A polycrystalline BiOI electrode, composed of extremely thin 2D plates, allowed for the preparation of porous $BiVO_4$ photoanodes using a simple chemical and thermal treatment. The resulting $BiVO_4$ with high porosity showed outstanding PEC efficiency. On the basis of these results, Kim and Choi[48] modified a previous synthesis developed by McDonald and Choi.[51] It is possible to facilitate the production of nanoporous $BiVO_4$, as displayed in Fig. 7(a)-(f), which is composed of much smaller particles, achieving an enlarged surface area.[48] The major change was the solution used as the source for conversion of BiOI to $BiVO_4$. They observed that the surface of BiOI film is highly hydrophobic; thus the aqueous vanadium solution used in the study by McDonald and Choi could not easily penetrate into the $BiVO_4$ films. As a result, the conversion of BiOI to $BiVO_4$ was initiated only at the top of the film surface, and the grains of $BiVO_4$ grew toward the bottom of the film by slow solid-state diffusion, resulting in the formation of large particles of $BiVO_4$ and no porosity in that direction, limiting the surface area. When the aqueous vanadium solution was replaced by a more hydrophobic DMSO solution containing vanadyl acetylacetonate as the vanadium source, the solution could easily penetrate the entire BiOI film. Therefore, upon heating, multiple nuclei could form, even within a single BiOI sheet, resulting in the formation of smaller particles, which considerably increased the porosity and the surface area. This research proposed a novel technique of electrochemical deposition and demonstrated that nanoporous morphology with high surface area effectively suppresses carrier recombination without additional doping.

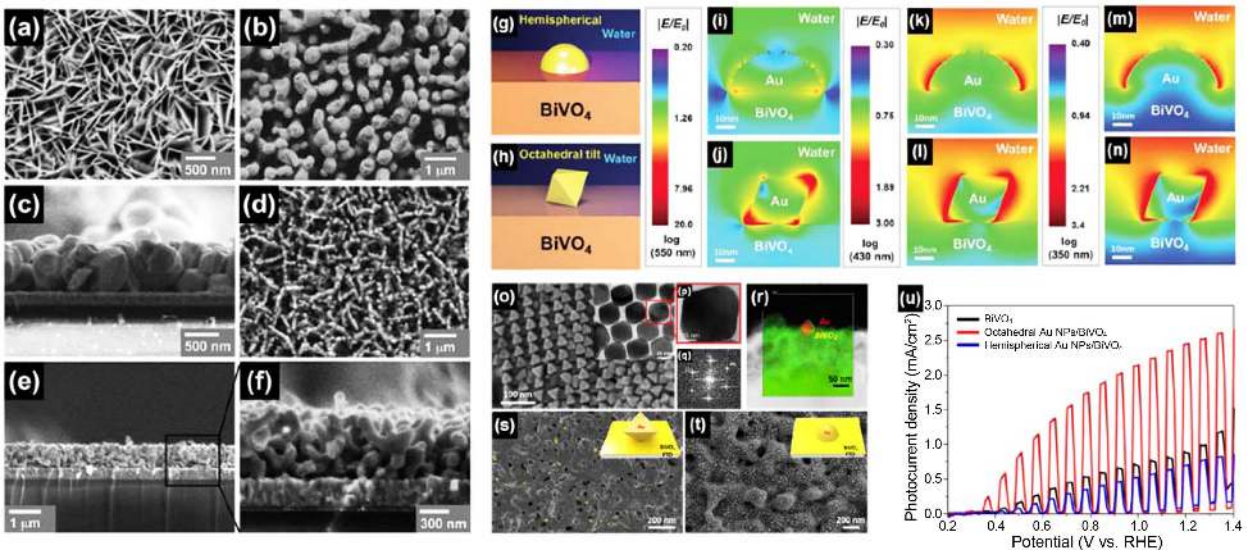

Fig. 7. (a) SEM images for nanoporous (a) BiOI films. (b), (c) Top view and cross-section view of $BiVO_4$ film fabricated by NH_4OH/V_2O_5 and (d)-(f) top view and cross-section view of $BiVO_4$ film fabricated by $DMSO/VO(acac)_2$. Adapted with permission from Ref 48. (g)-(n) Schematic representation of finite-difference time-domain (FDTD) configurations for hemispherical and octahedral Au NPs on $BiVO_4$ film under different wavelength of photon, respectively. (o) SEM, (p) TEM images and (q) FFT pattern of octahedral Au NPs and (r) EDS result of octahedral NPs on $BiVO_4$ film by mapping. False color SEM image of (s) octahedral Au NPs on $BiVO_4$ film and (t) hemispherical Au NPs on $BiVO_4$ film. (u) LSV curve of each $BiVO_4$ film. Adapted with permission from Ref 5.

Another approach to improve absorbance and charge separation efficiency of $BiVO_4$ is shown in Fig. 7(g)-(u). Lee *et al.*[5] first introduced shape-controlled gold nanoparticles (Au NPs) as plasmonic NPs on $BiVO_4$ thin film synthesized by pulsed electrodeposition. They reported shape-controlled Au NPs with optimum coverage that significantly promote the photoactivity of $BiVO_4$ in over-band gap photon energy, rather than sub-band gap photon energy. Well-defined octahedral Au NPs significantly increased photocurrent density of $BiVO_4$ about 3-fold, while hemispherical Au NPs reduced it, since largely-enhanced localized surface plasmon resonance electric fields (LSPR-EFs) are only observed with octahedral Au NPs. Finite-domain time-difference (FDTD) simulation also validated intensified LSPR-EFs in the entire UV-vis region from octahedral Au NPs, compared to hemispherical Au NPs, indicating that control of the shape of plasmonic Au NPs is the key to achieving high PEC efficiency.

2.1.3. Tungsten oxide (WO_3)

In addition to homogeneous $BiVO_4$, the formation of type II heterojunctions has proven to be effective to facilitate the separation of photo-induced electron-hole pairs, enlarge the interfacial area, and maximize light absorption.[3] The combination of $BiVO_4$ and WO_3 to form a type II heterojunction not only facilitates charge separation, but also expands the light absorption capability of the composite photoelectrode.[3,11,26]

Jin *et al.* first designed a WO_3 thin film consisting of yolk-shell structured nanoparticles via a solution process without the use of vacuum deposition, as shown in Fig. 8(a)-(f).[53] A thin $BiVO_4$ layer with a smaller band gap was coated onto the surface of and inside the WO_3 shells, providing a rationally-designed inner space between the particles and the shell for better electrolyte accessibility. The yolk-shell-shaped PEC photoanode not only induces efficient light absorption but also plays an important role in electron collection from $BiVO_4$ due to an enlarged contact area. The photocurrent density of the yolk-shell (Y-WO_3/$BiVO_4$/OER) photoanode achieved its highest value of 5.0 mA/cm^2 at 1.23 V vs. RHE.

Lee *et al.*[3] reported highly ordered one-dimensional WO_3 nanorods by changing their porosity and aspect ratio, and depositing stoichiometric $BiVO_4$ on the surface of the WO_3 nanorods by pulsed electrodeposition. The notable point of this research is that cross-sectional transmission electron microscopy shows dot-like $BiVO_4$ well coated on the entire surface of the WO_3 nanorods. $BiVO_4$/WO_3 type II heterojunction anodes can lead to a high photocurrent density of 4.55 mA/cm^2 and an incident photon-to-current conversion efficiency of 80% at 1.23 V versus a reversible hydrogen electrode without additional catalyst.

Pihosh *et al.*[54] demonstrated this concept with a WO_3/$BiVO_4$+CoPi core-shell nanostructured photoanode that achieves near theoretical water splitting efficiency, as shown in Fig. 8(h)-(k). This study combines $BiVO_4$ with more conductive WO_3 nanorods in the form of a core-shell heterojunction, where the $BiVO_4$ absorber layer is thinner than the carrier diffusion length, while its optical thickness is re-established by light trapping in high aspect ratio nanostructures. Their photoanode demonstrates an ultimate water splitting photocurrent of 6.72 mA/cm^2 under 1 sun

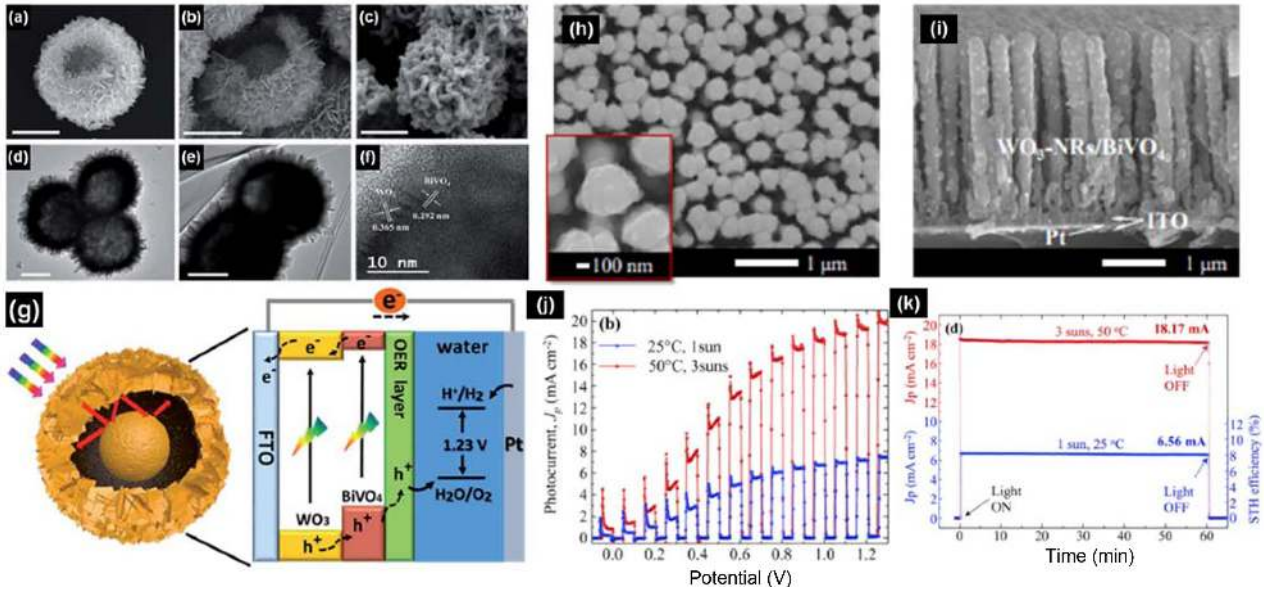

Fig. 8. SEM and TEM images of (a), (d) hollow WO_3, (b), (e) yolk-shell WO_3 and (c), (f) yolk-shell $WO_3/BiVO_4$ heterojunctions, respectively. (g) Schematic representation of the yolk-shell $WO_3/BiVO_4$ photoanode and expected energy band diagram. Adapted with permission from Ref 53. (h), (i) Top and cross-sectional SEM images of $BiVO_4$ coated on WO_3 nanorods. (j) Linear sweep voltammograms for WO_3-NRs/$BiVO_4$+CoPi photoanode measured under chopped light at 1 sun, 25°C and at 3 suns, 50°C. (k) J_p-t profiles measured for the PEC-PV tandem at 1 sun, 25°C (blue) and 3 suns, 50°C (red). Adapted with permission from Ref 54.

illumination at 1.23 V vs. RHE, which corresponds to ~ 90% of the theoretically possible value for $BiVO_4$.

2.1.4. Titanium dioxide (TiO_2)

Titanium dioxide (TiO_2) has been favored in many industrial fields for its excellent thermodynamic stability and chemical resistance.[55-59] In the case of photocatalytic applications, the discovery of photocatalytic phenomena of TiO_2 by Fujishima and Honda in 1972[60] demonstrated the potential for new applicable areas, i.e. photovoltaics and photocatalysts. Since then, considerable efforts have been made to make TiO_2 a promising material for photocatalysis,[55,61-65] and today TiO_2 is considered one of the potential candidates to play an important role in solving environmental and pollution problems as a photocatalyst. Following the innovative work of Fujishima and Honda, several synthetic methods including sol-gel,[66-70] chemical vapor deposition,[71-74] physical vapor deposition,[75-77] and others[78-81] have been adapted to synthesize TiO_2 photocatalysts. But most of these cases show a lower photocurrent density than other photoanodes because of a higher resistance and larger band gap (3.0 - 3.2 eV) for TiO_2.[82] Consequently, these disadvantages would need to be overcome in order to fabricate stable and efficient TiO_2 photoanodes. Several strategies have been proposed to maximize the potential of TiO_2 as a photoanode, and these will be further discussed here.

One approach to overcome the limit of TiO_2 photocatalysts is reinforcement of photon absorption and reaction with electrolytes by increasing surface area to volume ratio,[83] and formation of nanostructure is always a good choice to maximize the surface area of films. Some researchers have synthesized TiO_2 nanostructure arrays by coating on different nanostructured templates such as anodic alumina membrane (AAM) and ZnO.

In 2003, Lin *et al.*[84] fabricated TiO_2 nanowire arrays by electrophoretic deposition into the pores of an AAM. Colloidal suspensions for electrophoretic deposition of TiO_2 were synthesized by dissolving titanium tetraisopropoxide (TTIP) in ethanol and mixing with glacial acetic acid solution and the addition of nitric acid to adjust the pH to 2 - 3. An AAM with an Au substrate attached to Cu foil was used as a cathode, and platinum was used as an anode. The deposition condition for the TiO_2 coating into the pores of the AAM was a voltage of 2 - 5 V and fabricated films were annealed at 500°C for 24 h. Isolated TiO_2 nanowires could be obtained after dissolving the AAM templates in a 5 wt% NaOH solution. The length of the nanowires was dependent on the length of the AAM pores.

TiO_2 nanotubes can be fabricated using the sol-gel method and AAM templates. Lee *et al.* in 2004[85] dipped an AAM template into a TTIP solution prepared by mixing TTIP with 2-propanol and 2,4-pentanedione, and the sol-coated template was placed under vacuum until the entire volume of the solution was pulled through the AAM. The AAM was hydrolyzed by water vapor over HCl solution for 24 h, air-dried at room temperature, and then calcined at 400°C for 2 h and cooled to room temperature at a cooling rate of 2°C/h. Pure TiO_2 nanotubes were obtained after the AAM was dissolved in 6 M NaOH for several min. TiO_2 nanotubes could also be obtained by a chemical bath deposition method

using AAM. Reported by Liu *et al.*,[86] TiO_2 nanotubes could be synthesized by simply submerging AAM template in dilute TiF_4 at pH 2.1 and 60°C for 12 - 48 h.

Not only AAM, but also a ZnO nanorod array on glass substrate could be used as a TiO_2 nanotube template. Similarly, TiO_2 nanotube arrays could be obtained by etching ZnO in a ZnO nanorod template coated with TiO_2 by a dip-coating method.[87] Dilute HCl was used as an etchant for the ZnO nanorods and, due to the structure of the ZnO building unit, the TiO_2 nanotubes had pores with a hexagonal shape.

In order to make TiO_2 films as photoelectrodes, it is necessary to generate a junction with a conductive substrate. However, a difference of refractive index between TiO_2 and the substrate induces a reflection of incident light which reduces light absorption.[88] To overcome this phenomenon, some researchers adapted the characteristics of a rutile TiO_2 growth unit. As the crystal planes of TiO_2 have quite different surface energies, rutile TiO_2 shows preferential crystal growth when synthesized by a hydrothermal process.[56,89-91] Using this method, fabrication of a branched nanorod structure has been tried. Cho *et al.*[92] fabricated branched nanorod TiO_2 films on a FTO substrate by a two-step synthesis. First, TiO_2 nanorods were grown hydrothermally on TiO_2-coated FTO substrate. Tetrabutyl titanate (TBT), 25 mL of deionized (DI) water, and 25 mL of concentrated HCl were stirred to create a hydrothermal solution. The obtained TiO_2 nanorods films were annealed at 450°C for 1 h in air, and seed nanoparticles for TiO_2 branches were deposited by a dip-coating method using the TiO_2 polymeric solution. The seeded nanorods films were immersed in an aqueous solution consisting of 10 mL of DI water, 0 - 0.5 mL of HCl, and 0.1 mL of $TiCl_3$ solution and kept at 80°C for 1 - 2 h. Finally, branched nanorod films were obtained by washing with ethanol and annealing at 450°C for 1 h in air. The obtained nanorods and branched nanorods showed much lower reflectance in the UV region compared with porous nanoparticles because of a change in film density from bottom to top and scattering of incident light.[88]

Such examples for controlling TiO_2 nanostructure have contributed to enormous advances over simple planar thin films, but still further enhancements are needed before TiO_2 photoanodes can be commercialized. Based on the belief that research on single TiO_2 structures has reached its theoretical upper limit, co-catalyst attached TiO_2 photoanodes have been examined recently. Among these, the Au nanoparticle-coated TiO_2 branched nanorod structure, reported by Su *et al.*,[93] shows outstanding results. A schematic of the experimental procedure for preparing these nanorods is illustrated in Fig. 9. Similar to the above case, TiO_2 nanorods were hydrothermally synthesized on FTO with a

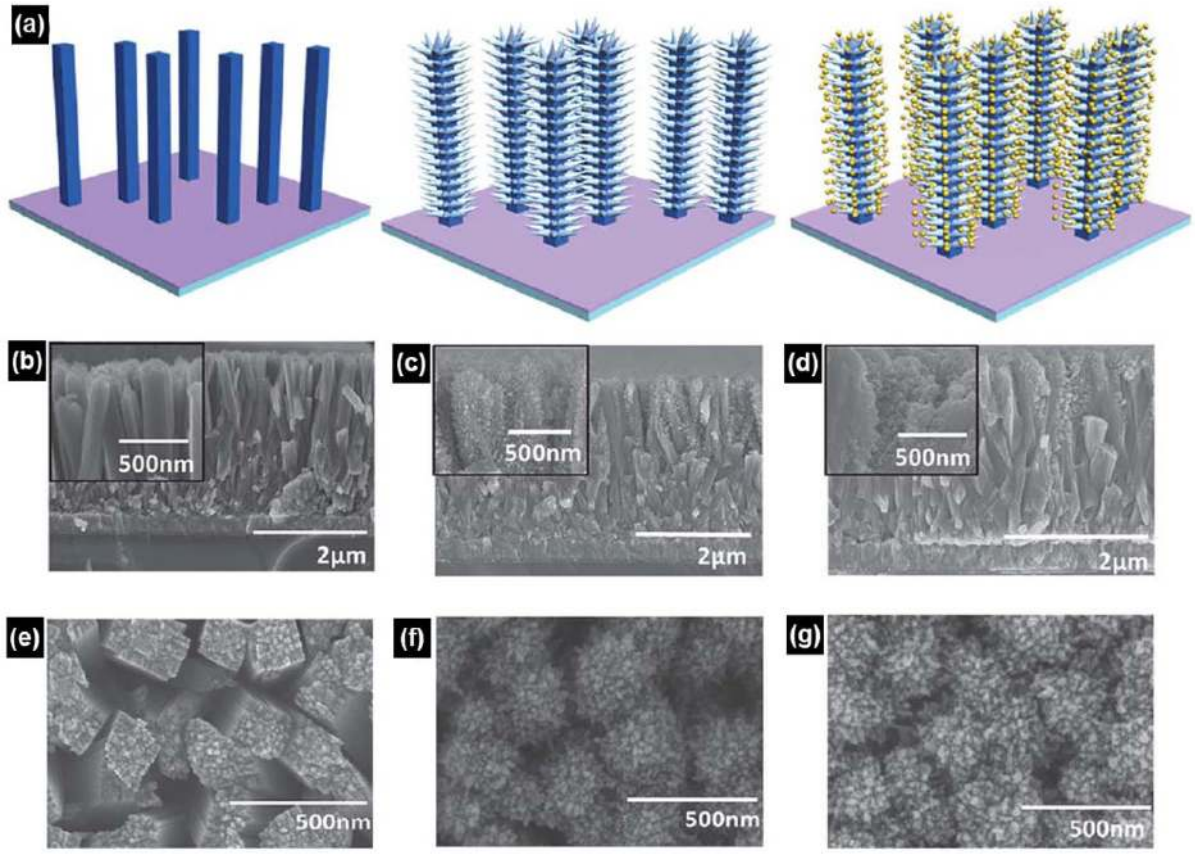

Fig. 9. (a) Schematic representation of the synthesis steps of Au coated TiO_2 branched nanorods (BNRs). Scanning electron micrographs of (b and e) TiO_2 NRs, (c and f) TiO_2 BNRs and (d and g) Au coated TiO_2 BNRs, respectively. Adapted with permission from Ref 93.

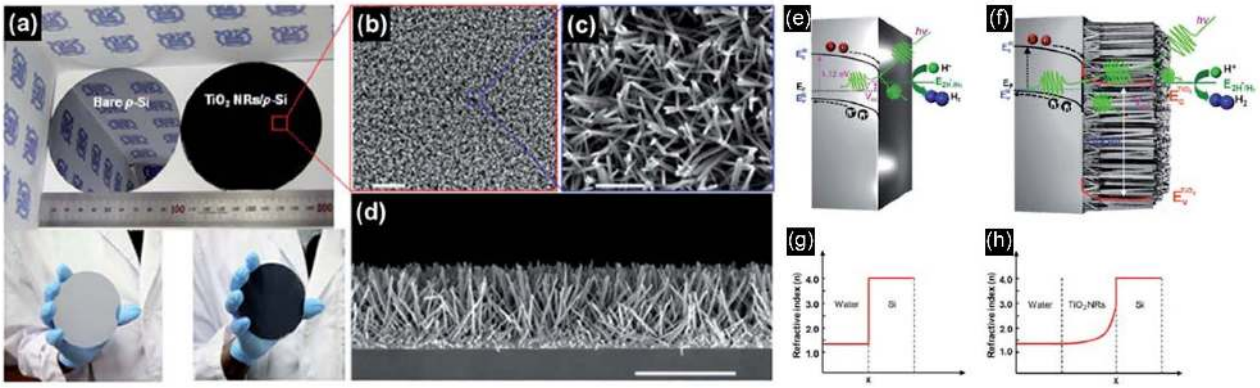

Fig. 10. (a) Optical image of bare p-Si (left) and hydrothermally grown TiO_2 NRs on p-Si (right). SEM images of corresponding TiO_2 NRs with (b) and (c) different magnification in top view and (d) cross-section view. Schematic representation of photoelectrodes and corresponding energy band diagrams under irradiation. Possible assumption of light attenuation for (g) electrolyte/p-Si and (h) electrolyte/TiO_2 NRs/p-Si system. Adapted with permission from Ref 88.

solution composed of 30 mL of DI water, 30 mL of concentrated HCl, 1 mL of TBT and 5 mL of 5 M NaCl. Hydrothermally prepared TiO_2 nanorods were immersed in 0.2 M $TiCl_4$ at room temperature for 18 h and then rinsed with absolute ethanol. Specimens were annealed at 450°C for 30 min. The fabricated TiO_2 branched nanorods were immersed in 0.3 mM $HAuCl_4$, dispersed in DI water, and irradiated with a 300 W Xe lamp for 6 h to coat Au nanoparticles on TiO_2 surfaces. The much higher photocurrent density shown in this study demonstrates that both strategies, i.e. increasing surface area and enhancing surface reaction by a co-catalyst, can be successfully adopted at the same time.

Recently it has been shown that the use of TiO_2 can be extended to photocathodes as well as photoanodes. Andoshe *et al.*[88] fabricated a photocathode with a heterojunction of p-Si and TiO_2 nanorod thin film. For the heterogeneous nucleation of TiO_2 nanorods during hydrothermal synthesis, a 5 nm thick seed layer of the TiO_2 film was deposited on p-Si. Subsequently, TiO_2 nanorods were hydrothermally grown on a seed layer of deposited p-Si substrate at 180 - 220°C for 0.5 - 2 h. The solution for the hydrothermal process contained 25 mL of DI water, 25 mL of concentrated HCl and 0.8 mL of TBT. As shown in Fig. 10(a), the TiO_2 nanorod/p-Si photocathode exhibits a matt black color. As illustrated in Fig. 10(b)-(h), a gradual change in nanorod density along the vertical direction causes a steady change of refractive index that restricts total reflection. TiO_2 has the additional role of passivating p-Si from corrosion. Likewise, TiO_2 exhibits a potential for heterojunction, passivation, and interface modulation materials.

2.2. Photocathodes

Despite significant efforts over the past decades to develop new photocathode materials for solar hydrogen production via water splitting, there are only a few metal oxide based photocathodes, such as copper-based oxides, that can meet the requirements for commercially viable solar water splitting.[8,94-95] Two long-standing bottlenecks for metal oxide photocathodes are sensitivity to photocorrosion during the hydrogen production process and low quantum efficiencies. Here, we review recent developments using metal oxide-based photocathodes synthesized by a solution process for efficient and stable water splitting.

2.2.1. Cuprous oxide (Cu_2O) and Copper oxide (CuO)

Cu_2O and CuO are the most representative p-type binary oxides that have been introduced for use in solar water splitting. In addition to their favorable band gap energies that allow for the utilization of visible light, the low cost, earth abundance, and non-toxicity of Cu are additional advantages for developing Cu-based photoelectrodes.[94]

Cu_2O, with a direct band gap of 2.0 eV, is an attractive oxide for solar water reduction, thus it is possible to theoretically reach a photocurrent of 14.7 mA/cm^2 and a solar to hydrogen efficiency of 18%. The major limitation of Cu_2O is photocorrosion (e.g., $Cu_2O + 2H^+ + 2e^- \rightarrow 2Cu + H_2O$).[96] Paracchino *et al.*[97] successfully synthesized Cu_2O films by using electrochemical deposition, which was produced by cathodic reduction of Cu^{2+} ions in an aqueous alkaline (pH 12) solution. Cu_2O grains were covered with metal oxide protective layers [5 × (4 nm ZnO/0.17 nm Al_2O_3)/11 nm TiO_2] via atomic layer deposition (ALD), and finally coated with Pt nanoparticles, resulting in outstanding film quality when coated by ALD. Significantly, the protected Cu_2O photocathode exhibited substantially improved photoactivity and stability. The surface-protected Cu_2O achieved a photocurrent density of − 7.6 mA cm^{-2} under AM 1.5 illumination; furthermore, the protected electrodes remained photoactive after 1 h of testing and the measured Faradaic efficiency was close to 100%.

Yang *et al.*[95] demonstrated a Cu_2O/CuO bilayer composite synthesized by a facile method that involved electrodeposition and a subsequent thermal oxidation, as shown in Fig. 11(a)-(d). This strategy of combining electrodeposition and thermal oxidation provides an easy, low cost, and scalable strategy to prepare Cu_2O/CuO heterogeneous photocath-

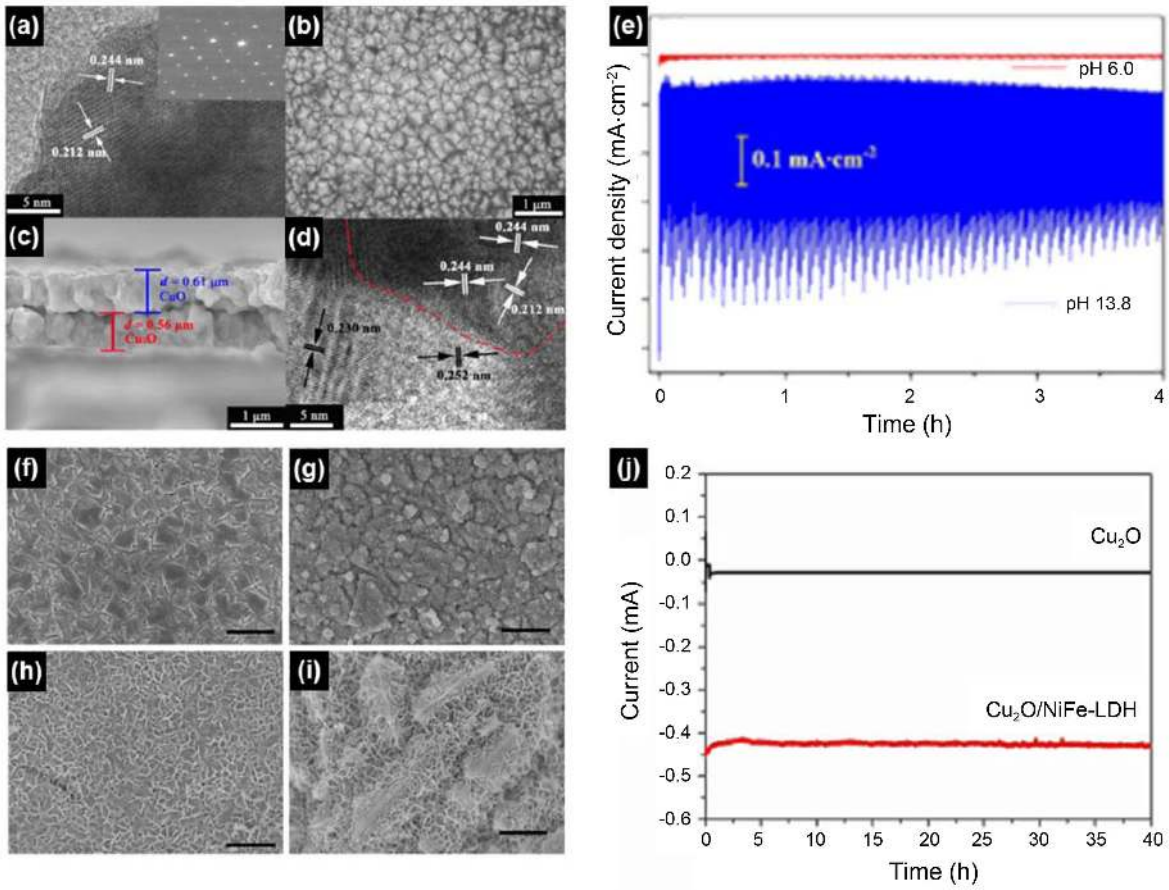

Fig. 11. (a) HRTEM image and SAED pattern (inset) of Cu_2O. (b) Top view and (c) cross-section view SEM images and (d) HRTEM image of Cu_2O/CuO bilayered composite. (e) Stability of Cu_2O/CuO bilayered composite with different pH values at 0.76 V vs. RHE. Adapted with permission from Ref 95. (f)-(i) SEM images of Cu_2O/NiFe-LDH with different electrodeposition times from 20 to 300 s. (j) Stability of Cu_2O and Cu_2O/NiFe-LDH at − 0.2 V vs Ag/AgCl. Adapted with permission from Ref 94.

odes for HER. The Cu_2O/CuO photocathode exhibited significantly high photoactivity and good photostability toward HER, especially at high potentials in alkaline solution. The photocurrent density for HER was 3.15 mA/cm^2 at a potential of 0.40 V vs. RHE, which was one of the highest reported values at the same potential on copper-oxide-based photocathodes. Good photostability was seen during the 4 h measurements.

Qi *et al.*[94] introduced NiFe-layered double hydroxide (NiFe-LDHs) overlayers as co-catalyst on Cu_2O electrodes via electrodeposition and studied their PEC behavior, as shown in Fig. 11(f)-(j). The electrodeposition enabled the synthesis of uniformly-anchored NiFe-LDH layered nanoplates onto the Cu_2O surface. The resulting Cu_2O/NiFe-LDH exhibited a remarkable 7-fold enhancement of photocurrent density under an applied voltage as low as − 0.2 V vs. Ag/AgCl. Also, long-term photostability tests revealed that Cu_2O/NiFe-LDH photocathodes showed no photocurrent loss after 40 h of operation under light at − 0.2 V vs Ag/AgCl low bias condition, which makes Cu_2O/NiFe-LDH photocathode a good candidate for low bias PEC water splitting.

CuO is another well-known photocathode with an indirect band gap of 1.2 - 1.8 eV. Due to its smaller band gap, it is possible to achieve a higher photocurrent than with Cu_2O, but CuO has received less attention than Cu_2O for use as a photocathode in solar water splitting. This lack of attention is probably because of uncertainty as to whether the photoexcited electrons in CuO could reduce water to H_2 (the conduction band minimum of CuO is reported to be between 0 and − 0.2 V vs RHE, which is more positive than that of Cu_2O).[98] Also, photocorrosion of CuO is another limiting factor for use in PEC water splitting. Recent studies showed suppressed photocorrosion of CuO.[98-99]

Cardiel *et al.*[100] developed novel electrochemical synthesis methods to produce copper hydroxyl double salt (Cu-HDS) films with four different intercalated anions (NO^{3-}, SO_4^{2-}, Cl^-, and dodecyl sulfate) as pure crystalline films, deposited as ($Cu_2NO_3(OH)_3$, $Cu_4SO_4(OH)_6$, $Cu_2Cl(OH)_3$, and $Cu_2DS(OH)_3$), as shown in Fig. 12. These methods are based on p-benzoquinone reduction, which increases the local pH at the working electrode and triggers the precipitation of Cu^{2+} and appropriate anions as Cu-HDS films on the working elec-

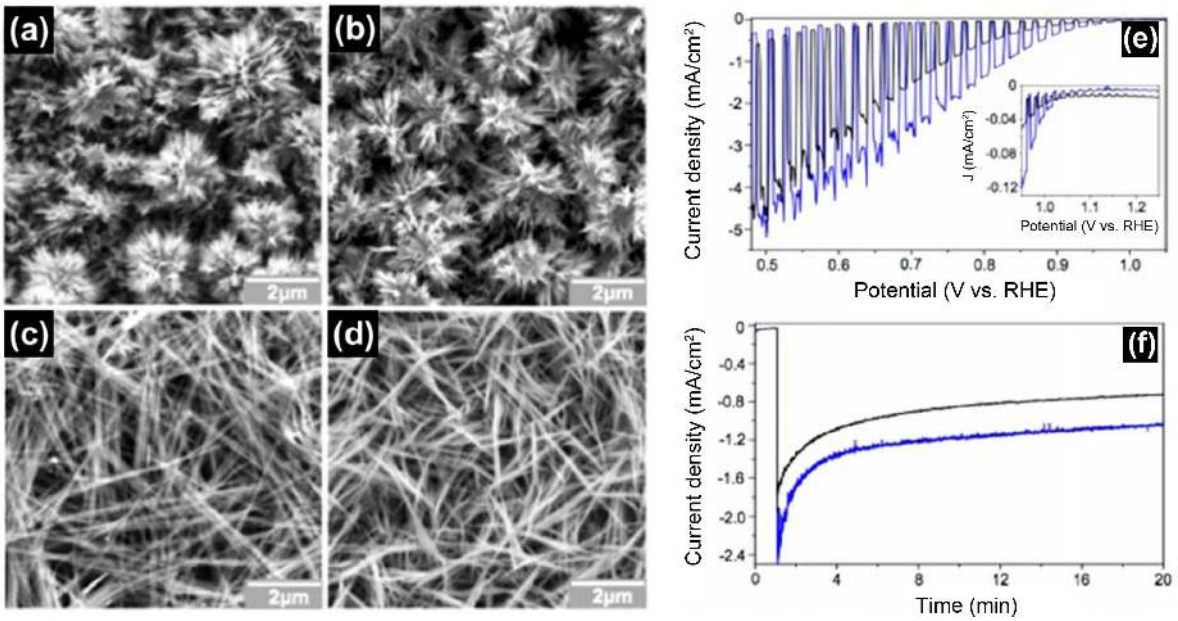

Fig. 12. SEM images of various copper oxide films originating from Cu-HDS/SO_4^{2-} films; (a) After soaking in pH 12 solution at 60°C for 2 h (CuO I) and (b) after heat treatment of (a) at 500°C for 3 h (CuO II). (c) After immersion in 1 M NaOH for 15 s and (d) after heat treatment of (c) at 500°C for 3 h.(CuO III) (e) LSV curve of CuO I (red line), CuO II (blue line) and Cu III (black line) under AM 1.5G (100 MW/cm^2) illumination with chopped light condition. (f) Plot of current density vs. time at 0.7 V vs. RHE for CuO II (blue line) and CuO III (black line) under AM 1.5G (100 MW/cm^2) illumination. Adapted with permission from Ref 100.

trode. The resulting Cu-HDS films could be converted to crystalline $Cu(OH)_2$ and CuO films by immersing them in basic solutions. The CuO films prepared from Cu-HDS films have unique low-dimensional nanostructures, creating high surface areas that cannot be obtained by direct deposition of CuO, which has a 3D atomic-level crystal structure, since Cu-HDS films were composed of 2D crystals as a result of the atomic-level layered structure of HDS. The CuO films recorded great onset potential (> 1.0 V vs RHE) very close to their flat band potential (~ 1.2 V vs RHE), which shows

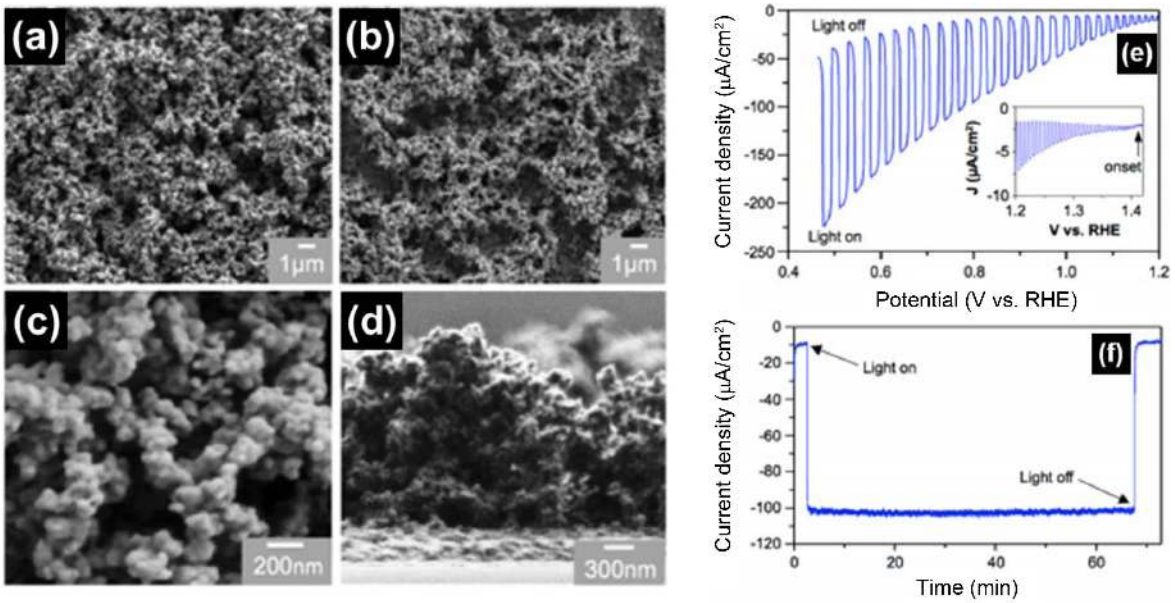

Fig. 13. SEM images of (a) an as-deposited La-Fe-O film with top view and (b-d) an annealed LaFeO3 film with top view and cross-section view, respectively. (e) LSV curve of $LaFeO_3$ film under AM 1.5G (100 MW/cm^2) illumination with chopping light condition and (f) J-t plot of $LaFeO_3$ film at 0.75 V vs. RHE of $LaFeO_3$ under AM 1.5G (100 MW/cm^2) illumination. Adapted with permission from Ref 103.

great promise for use as photocathodes in PEC cells for solar water splitting.

2.2.2. Other Metal Oxides as Photocathode

To date, metal oxides as photocathodes have been focused primarily on Cu-based oxides such as Cu_2O, CuO, $CuFeO_2$ and $CuBi_2O_4$.[28,101-102] However, the presence of copper in most p-type oxides is known to be a cause for photocorrosion, therefore these materials need a protection layer. Recent studies have searched for a breakthrough to solve the limitations of Cu-based metal oxides as photocathodes.

Perovskite-type lanthanum iron oxide ($LaFeO_3$) is a p-type oxide that has several attractive characteristics such as an ideal band gap of 2.1 eV and band edger positions for use in PEC water splitting. Wheeler *et al.*[103] reported nanoporous $LaFeO_3$ prepared by electrochemical co-deposition of $La(OH)_3$ and $Fe(OH)_2$ via nitrate reduction, as shown in Fig. 13. The significant finding of this study is that, after 1 h of PEC measurement for water reduction at 0.5 V vs. RHE, there is a negligible portion of surface electrons being used for water reduction, and no sign of photocorrosion unlike Cu-based metal oxides. This confirmed that $LaFeO_3$ is a rare p-type oxide that does not suffer from photocorrosion. Therefore, the enhancement of the PEC performance of $LaFeO_3$ can be expected with systematic doping studies and by combining it with a proper hydrogen catalyst.

3. Perspective and Outlook

Based on the previous discussion, we have reported the most recent progress of solution-based metal oxides for PEC water splitting. Even though metal oxide materials have substantial potential as photoelectrodes, there remain a number of challenges that need to be overcome. Poor electrical conductivity, limited light absorption, and photocorrosion are still the main drawbacks of most metal oxides when used as photoelectrodes for PEC water splitting. Thus, various strategies have been introduced to solve these limitations and improve the PEC performance of metal oxides. These strategies include the formation of nanostructures, band structure modification, introduction of plasmonic nanoparticles, the formation of heterostructures, and co-catalyst modification, in order to increase light absorption and enhance charge transfer. The following are some suggestions for future research directions along with their challenges, to improve PEC water splitting and possibly lead to breakthroughs.

The formation of nanostructures such as nanoparticles, nanotubes, nanorods, nanocorals, and nanotrees is a promising approach to enhance photoactivity. Morphology control provides an effective pathway for charge transport and to significantly suppress electron-hole recombination. Most of all, 3-dimensional (3D) net structures can not only provide more active sites for solar water splitting, but also facilitate charge transport and collection. The suggested solution processes have great potential to synthesize uniform 3D nanostructures and enable conformal deposition on various 1D nanostructures. The formation of type II heterojunctions has been recognized as an attractive route to promote efficient charge separation, which enlarges the interfacial area and improves optical absorption, thus it is crucial to find the best junction materials. Modification of band structure is a powerful approach to modify electronic structure and surface structure. The proper configuration and distribution of foreign dopants in semiconductor materials can optimize their electronic structures for efficient harvesting of sunlight.[104,105] Co-catalysts have played a critical role in the solar water splitting reaction,[106] such as reducing charge recombination, increasing reaction kinetics, and protecting materials from chemical corrosion, thus it is necessary to develop co-catalysts with cost-effective and superior properties. Plasmonic nanoparticles can increase the photocurrent density of metal oxides to exceed theoretical values, since three critical enhancement factors of plasmonics: hot electron injection, plasmonic resonance energy transfer, and scattering, can simultaneously operate. A further research field in PEC water splitting is to develop a suitable technology for large scale photoelectrode fabrication and cost-effective solar fuel production to compete with fossil fuel. All of the above strategies for developing efficient solar water splitting system can be satisfied by solution processes. Solution processes such as hydrothermal and electrodeposition facilitate the synthesis of uniform and 3D nanostructures by controlling parameters and enabling large-scale synthesis without restriction of electrode size. When considered together, it is clear that solution-based methods are a very promising pathway for cost-effective PEC cell fabrication systems.

In this article, we have reviewed recent progress in the field of nanostructured metal oxides synthesized by solution processes for PEC water splitting. We divided metal oxides into photoanodes and photocathodes. Unlike many impressive results that have been achieved in the use of metal oxides as photoanodes, research on metal oxides as photocathodes is markedly insufficient. In the future, it is necessary to find good candidates for photocathodes to make overall progress in PEC water splitting systems. Thus we believe that, besides improving the performance of existing metal oxide semiconductors, searching new metal oxide materials with highly efficient photocatalytic activity is also of crucial importance for PEC water splitting.

Acknowledgments

This research was supported by the Basic Science Research Program through the National Research Foundation of Korea (NRF) funded by the Ministry of Science, ICT & Future Planning (2017R1A2B3009135).

REFERENCES

1. X. Li, J. Yu, J. Low, Y. Fang, J. Xiao, and X. Chen, "Engi-

neering Heterogeneous Semiconductors for Solar Water Splitting," *J. Mater. Chem. A,* **3** [6] 2485-534 (2015).
2. J. Gan, X. Lu, and Y. Tong, "Towards Highly Efficient Photoanodes: Boosting Sunlight-Driven Semiconductor Nanomaterials for Water Oxidation," *Nanoscale,* **6** [13] 7142-64 (2014).
3. M. G. Lee, D. H. Kim, W. Sohn, C. W. Moon, H. Park, S. Lee, and H. W. Jang, "Conformally Coated $BiVO_4$ Nanodots on Porosity-Controlled WO_3 Nanorods as Highly Efficient Type II Heterojunction Photoanodes for Water Oxidation," *Nano Energy,* **28** 250-60 (2016).
4. Z.-F. Huang, L. Pan, J.-J. Zou, X. Zhang, and L. Wang, "Nanostructured Bismuth Vanadate-Based Materials for Solar-Energy-Driven Water Oxidation: A Review on Recent Progress," *Nanoscale,* **6** [23] 14044-63 (2014).
5. M. G. Lee, C. W. Moon, H. Park, W. Sohn, S. B. Kang, S. Lee, K. J. Choi, and H. W. Jang, "Dominance of Plasmonic Resonant Energy Transfer over Direct Electron Transfer in Substantially Enhanced Water Oxidation Activity of $BiVO_4$ by Shape-Controlled Au Nanoparticles," *Small*, **13** [37] 1701644 (2017).
6. C. Jiang, S. J. Moniz, A. Wang, T. Zhang, and J. Tang, "Photoelectrochemical Devices for Solar Water Splitting-Materials and Challenges," *Chem. Soc. Rev.*, **46** [15] 4645-60 (2017).
7. T. Hisatomi and K. Domen, "Introductory Lecture: Sunlight-Driven Water Splitting and Carbon Dioxide Reduction by Heterogeneous Semiconductor Systems as Key Processes in Artificial Photosynthesis," *Faraday Discuss.,* **198** 11-35 (2017).
8. Y. Yang, S. Niu, D. Han, T. Liu, G. Wang, and Y. Li, "Progress in Developing Metal Oxide Nanomaterials for Photoelectrochemical Water Splitting," *Adv. Energy Mater.,* **7** [19] 1700555 (2017).
9. I. D. Sharp, J. K. Cooper, F. M. Toma, and R. Buonsanti, "Bismuth Vanadate as a Platform for Accelerating Discovery and Development of Complex Transition-Metal Oxide Photoanodes," *ACS Energy Lett.,* **2** [1] 139-50 (2016).
10. H. M. Chen, C. K. Chen, R.-S. Liu, L. Zhang, J. Zhang, and D. P. Wilkinson, "Nano-Architecture and Material Designs for Water Splitting Photoelectrodes," *Chem. Soc. Rev.*, **41** [17] 5654-71 (2012).
11. H. Wang, L. Zhang, Z. Chen, J. Hu, S. Li, Z. Wang, J. Liu, and X. Wang, "Semiconductor Heterojunction Photocatalysts: Design, Construction, and Photocatalytic Performances," *Chem. Soc. Rev.*, **43** [15] 5234-44 (2014).
12. M. G. Lee and H. W. Jang, "Photoactivities of Nanostructured α-Fe_2O_3 Anodes Prepared by Pulsed Electrodeposition," *J. Korean Ceram. Soc.,* **53** [4] 400-5 (2016).
13. J. Choi, J. T. Song, H. S. Jang, M.-J. Choi, D. M. Sim, S. Yim, H. Lim, Y. S. Jung, and J. Oh, "Interfacial Band-Edge Engineered TiO_2 Protection Layer on Cu_2O Photocathodes for Efficient Water Reduction Reaction," *Electron. Mater. Lett.,* **13** [1] 57-65 (2017).
14. K. S. Choi, H. S. Jang, C. M. McShane, C. G. Read, and J. A. Seabold, "Electrochemical Synthesis of Inorganic Polycrystalline Electrodes with Controlled Architectures," *MRS Bull.,* **35** [10] 753-60 (2010).
15. X. B. Chen, S. H. Shen, L. J. Guo, and S. S. Mao, "Semiconductor-Based Photocatalytic Hydrogen Generation," *Chem. Rev.,* **110** [11] 6503-70 (2010).
16. Y. Tachibana, L. Vayssieres, and J. R. Durrant, "Artificial Photosynthesis for Solar Water-Splitting," *Nat. Photonics,* **6** [8] 511-18 (2012).
17. K. Maeda and K. Domen, "Photocatalytic Water Splitting: Recent Progress and Future Challenges," *J. Phys. Chem. Lett.,* **1** [18] 2655-61 (2010).
18. M. Vaseem, A. Umar, S. H. Kim, and Y.-B. Hahn, "Low-Temperature Synthesis of Flower-Shaped CuO Nanostructures by Solution Process: Formation Mechanism and Structural Properties," *J. Phys. Chem. C,* **112** [15] 5729-35 (2008).
19. G. H. A. Therese and P. V. Kamath, "Electrochemical Synthesis of Metal Oxides and Hydroxides," *Chem. Mater.,* **12** [5] 1195-204 (2000).
20. K. Byrappa and M. Yoshimura, Handbook of Hydrothermal Technology; William Andrew, 2012.
21. N. Liu, X. Chen, J. Zhang, and J. W. Schwank, "A Review on TiO_2-based Nanotubes Synthesized via Hydrothermal Method: Formation Mechanism, Structure Modification, and Photocatalytic Applications," *Catal. Today,* **225** 34-51 (2014).
22. C. J. Brinker and G. W. Scherer, Sol-Gel Science: The Physics and Chemistry of Sol-Gel Processing; Academic Press, 2013.
23. Y.-H. Kim, J.-S. Heo, T.-H. Kim, S. Park, M.-H. Yoon, J. Kim, M. S. Oh, G.-R. Yi, Y.-Y. Noh, and S. K. Park, "Flexible Metal-Oxide Devices Made by Room-Temperature Photochemical Activation of Sol–Gel Films," *Nature,* **489** [7414] 128-32 (2012).
24. S. Gorer and G. Hodes, "Quantum Size Effects in the Study of Chemical Solution Deposition Mechanisms of Semiconductor Films," *J. Phys. Chem.,* **98** [20] 5338-46 (1994).
25. M. G. Walter, E. L. Warren, J. R. McKone, S. W. Boettcher, Q. X. Mi, E. A. Santori, and N. S. Lewis, "Solar Water Splitting Cells," *Chem. Rev.,* **110** [11] 6446-73 (2010).
26. S. J. Moniz, S. A. Shevlin, D. J. Martin, Z.-X. Guo, and J. Tang, "Visible-Light Driven Heterojunction Photocatalysts for Water Splitting-a Critical Review," *Energy Environ. Sci.,* **8** [3] 731-59 (2015).
27. C. X. Kronawitter, L. Vayssieres, S. Shen, L. Guo, D. A. Wheeler, J. Z. Zhang, B. R. Antoun, and S. S. Mao, "A Perspective on Solar-Driven Water Splitting with All-Oxide Hetero-Nanostructures," *Energy Environ. Sci.,* **4** [10] 3889-99 (2011).
28. D. Kang, T. W. Kim, S. R. Kubota, A. C. Cardiel, H. G. Cha, and K. S. Choi, "Electrochemical Synthesis of Photoelectrodes and Catalysts for Use in Solar Water Splitting," *Chem. Rev.,* **115** [23] 12839-87 (2015).
29. Z. W. Seh, J. Kibsgaard, C. F. Dickens, I. Chorkendorff, J. K. Nørskov, and T. F. Jaramillo, "Combining Theory and Experiment in Electrocatalysis: Insights into Materials Design," *Science,* **355** [6321] eaad4998 (2017).
30. T. Lindgren, L. Vayssieres, H. Wang, and S.-E. Lindquist, "Photo-Oxidation of Water at Hematite Electrodes," *Chem. Phys. Nanostruct. Semicond.,* 83-110 (2003).
31. H. Tsubomura, N. Yamamoto, N. Matsuo, and Y. Okada,

"The Visible Absorption Spectrum of Water," *Proc. Jpn. Acad., Ser. B,* **56** [7] 403-7 (1980).
32. K. L. Hardee and A. J. Bard, "Semiconductor Electrodes V. The Application of Chemically Vapor Deposited Iron Oxide Films to Photosensitized Electrolysis," *J. Electrochem. Soc.,* **123** [7] 1024-26 (1976).
33. R. K. Quinn, R. Nasby, and R. Baughman, "Photoassisted Electrolysis of Water Using Single Crystal α-Fe_2O_3 Anodes," *Mater. Res. Bull.,* **11** [8] 1011-17 (1976).
34. J. H. Kennedy, M. Anderman, and R. Shinar, "Photoactivity of Polycrystalline α-Fe_2O_3 Electrodes Doped with Group IVA Elements," *J. Electrochem. Soc.,* **128** [11] 2371-73 (1981).
35. C. Sanchez, K. Sieber, and G. Somorjai, "The Photoelectrochemistry of Niobium Doped α-Fe_2O_3," *J. Electroanal. Chem. Interfacial Electrochem.,* **252** [2] 269-90 (1988).
36. M. P. Dare-Edwards, J. B. Goodenough, A. Hamnett, and P. R. Trevellick, "Electrochemistry and Photoelectrochemistry of Iron (III) Oxide," *J. Chem. Soc., Faraday Trans. 1,* **79** [9] 2027-41 (1983).
37. J. H. Kennedy and K. W. Frese, "Photooxidation of Water at α-Fe_2O_3 Electrodes," *J. Electrochem. Soc.,* **125** [5] 709-14 (1978).
38. A. G. Joly, J. R. Williams, S. A. Chambers, G. Xiong, W. P. Hess, and D. M. Laman, "Carrier Dynamics in α-Fe_2O_3 (0001) Thin Films and Single Crystals Probed by Femtosecond Transient Absorption and Reflectivity," *J. Appl. Phys.,* **99** [5] 053521 (2006).
39. G. Horowitz, "Capacitance-Voltage Measurements and Flat-Band Potential Determination on Zr-Doped α-Fe_2O_3 Single-Crystal Electrodes," *J. Electroanal. Chem. Interfacial Electrochem.,* **159** [2] 421-36 (1983).
40. W. W. Gärtner, "Depletion-Layer Photoeffects in Semiconductors," *Phys. Rev.,* **116** [1] 84 (1959).
41. K. Itoh and J. O. M. Bockris, "Stacked Thin-Film Photoelectrode Using Iron Oxide," *J. Appl. Phys.,* **56** [3] 874-76 (1984).
42. K. Itoh and J. M. Bockris, "Thin Film Photoelectrochemistry: Iron Oxide," *J. Electrochem. Soc.,* **131** [6] 1266-71 (1984).
43. R. Gardner, F. Sweett, and D. Tanner, "The Electrical Properties of Alpha Ferric Oxide–II.: Ferric Oxide of High Purity," *J. Phys. Chem. Solids,* **24** [10] 1183-96 (1963).
44. K. Sivula, R. Zboril, F. L. Formal, R. Robert, A. Weidenkaff, J. Tucek, J. Frydrych, and M. Gratzel, "Photoelectrochemical Water Splitting with Mesoporous Hematite Prepared by a Solution-Based Colloidal Approach," *J. Am. Chem. Soc.,* **132** [21] 7436-44 (2010).
45. F. L. Souza, K. P. Lopes, P. A. Nascente, and E. R. Leite, "Nanostructured Hematite Thin Films Produced by Spin-Coating Deposition Solution: Application in Water Splitting," *Sol. Energy Mater. Sol. Cells,* **93** [3] 362-68 (2009).
46. J. Brillet, M. Gratzel, and K. Sivula, "Decoupling Feature Size and Functionality in Solution-Processed, Porous Hematite Electrodes for Solar Water Splitting," *Nano Lett.,* **10** [10] 4155-60 (2010).
47. J. Y. Kim, D. H. Youn, K. Kang, and J. S. Lee, "Highly Conformal Deposition of an Ultrathin FeOOH Layer on a Hematite Nanostructure for Efficient Solar Water Splitting," *Angew. Chem., Int. Ed.,* **55** [36] 10854-58 (2016).
48. T. W. Kim and K.-S. Choi, "Nanoporous $BiVO_4$ Photoanodes with Dual-Layer Oxygen Evolution Catalysts for Solar Water Splitting," *Science,* **343** [6174] 1245026 (2014).
49. F. E. Osterloh, "Inorganic Nanostructures for Photoelectrochemical and Photocatalytic Water Splitting," *Chem. Soc. Rev.,* **42** [6] 2294-320 (2013).
50. G. Xi and J. Ye, "Synthesis of Bismuth Vanadate Nanoplates with Exposed {001} Facets and Enhanced Visible-Light Photocatalytic Properties," *Chem. Commun.,* **46** [11] 1893-95 (2010).
51. K. J. McDonald and K.-S. Choi, "A New Electrochemical Synthesis Route for a BiOI Electrode and its Conversion to a Highly Efficient Porous $BiVO_4$ Photoanode for Solar Water Oxidation," *Energy Environ. Sci.,* **5** [9] 8553-57 (2012).
52. J. A. Seabold and K.-S. Choi, "Efficient and Stable Photo-Oxidation of Water by a Bismuth Vanadate Photoanode Coupled with an Iron Oxyhydroxide Oxygen Evolution Catalyst," *J. Am. Chem. Soc.,* **134** [4] 2186-92 (2012).
53. B. Jin, E. Jung, M. Ma, S. Kim, K. Zhang, J. I. Kim, Y. Son, and J. H. Park, "Solution-Processed Yolk-Shell-Shaped WO_3/$BiVO_4$ Heterojunction Photoelectrode for Efficient Solar Water Splitting," *J. Mater. Chem. A,* **2018** [6] 2585-92 (2018).
54. Y. Pihosh, I. Turkevych, K. Mawatari, J. Uemura, Y. Kazoe, S. Kosar, K. Makita, T. Sugaya, T. Matsui, and D. Fujita, "Photocatalytic Generation of Hydrogen by Core-Shell WO_3/$BiVO_4$ Nanorods with Ultimate Water Splitting Efficiency," *Sci. Rep.,* **5** 11141 (2015).
55. A. Fujishima, T. N. Rao, and D. A. Tryk, "Titanium Dioxide Photocatalysis," *J. Photochem. Photobiol., C,* **1** [1] 1-21 (2000).
56. U. Diebold, "The Surface Science of Titanium Dioxide," *Surf. Sci. Rep.,* **48** [5-8] 53-229 (2003).
57. X. Chen and S. S. Mao, "Titanium Dioxide Nanomaterials: Synthesis, Properties, Modifications, and Applications," *Chem. Rev.,* **107** [7] 2891-959 (2007).
58. M. Grätzel, "A Low-Cost, High-Efficiency Solar Cell Based on Dye-Sensitized Colloidal Titanium Dioxide Films," *Nature,* **353** 737-40 (1991).
59. Y. Matsumoto, M. Murakami, T. Shono, T. Hasegawa, T. Fukumura, M. Kawasaki, P. Ahmet, T. Chikyow, S.-Y. Koshihara, and H. Koinuma, "Room-Temperature Ferromagnetism in Transparent Transition Metal-Doped Titanium Dioxide," *Science,* **291** [5505] 854-56 (2001).
60. A. Fujishima and K. Honda, "Electrochemical Photolysis of Water at a Semiconductor Electrode," *Nature,* **238** [5358] 37-8 (1972).
61. O. Carp, C. L. Huisman, and A. Reller, "Photoinduced Reactivity of Titanium Dioxide," *Prog. Solid State Chem.,* **32** [1-2] 33-177 (2004).
62. X. Chen, L. Liu, Y. Y. Peter, and S. S. Mao, "Increasing Solar Absorption for Photocatalysis with Black Hydrogenated Titanium Dioxide Nanocrystals," *Science,* **331** [6018] 746-50 (2011).
63. T. Umebayashi, T. Yamaki, H. Itoh, and K. Asai, "Band Gap Narrowing of Titanium Dioxide by Sulfur Doping," *Appl. Phys. Lett.,* **81** [3] 454-56 (2002).

64. R. I. Bickley, T. Gonzalez-Carreno, J. S. Lees, L. Palmisano, and R. J. Tilley, "A Structural Investigation of Titanium Dioxide Photocatalysts," *J. Solid State Chem.,* **92** [1] 178-90 (1991).
65. M. Pelaez, N. T. Nolan, S. C. Pillai, M. K. Seery, P. Falaras, A. G. Kontos, P. S. Dunlop, J. W. Hamilton, J. A. Byrne, and K. O'shea, "A Review on the Visible Light Active Titanium Dioxide Photocatalysts for Environmental Applications," *Appl. Catal., B,* **125** 331-49 (2012).
66. Y. Bessekhouad, D. Robert, and J. V. Weber, "Synthesis of Photocatalytic TiO_2 Nanoparticles: Optimization of the Preparation Conditions," *J. Photochem. Photobiol., A,* **157** [1] 47-53 (2003).
67. K. D. Kim and H. T. Kim, "Synthesis of TiO_2 Nanoparticles by Hydrolysis of TEOT and Decrease of Particle Size Using a Two-Stage Mixed Method," *Powder Technolo.,* **119** [2-3] 164-72 (2001).
68. I. Kuznetsova, V. Blaskov, I. Stambolova, L. Znaidi, and A. Kanaev, "TiO_2 Pure Phase Brookite with Preferred Orientation, Synthesized as a Spin-Coated Film," *Mater. Lett.,* **59** [29-30] 3820-23 (2005).
69. J. H. Lee and Y. S. Yang, "Effect of HCl Concentration and Reaction Time on the Change in the Crystalline State of TiO_2 Prepared from Aqueous $TiCl_4$ Solution by Precipitation," *J. Eur. Ceram. Soc.,* **25** [16] 3573-78 (2005).
70. P. Liu, J. Bandara, Y. Lin, D. Elgin, L. F. Allard, and Y.-P. Sun, "Formation of Nanocrystalline Titanium Dioxide in Perfluorinated Ionomer Membrane," *Langmuir,* **18** [26] 10398-401 (2002).
71. S. Seifried, M. Winterer, and H. Hahn, "Nanocrystalline Titania Films and Particles by Chemical Vapor Synthesis," *Chem. Vap. Deposition,* **6** [5] 239-44 (2000).
72. J. Ayllon, A. Figueras, S. Garelik, L. Spirkova, J. Durand, and L. Cot, "Preparation of TiO_2 Powder Using Titanium Tetraisopropoxide Decomposition in a Plasma Enhanced Chemical Vapor Deposition (PECVD) Reactor," *J. Mater. Sci. Lett.,* **18** [16] 1319-21 (1999).
73. H. D. Jang and S.-K. Kim, "Controlled Synthesis of Titanium Dioxide Nanoparticles in a Modified Diffusion Flame Reactor," *Mater. Res. Bull.*, **36** [3-4] 627-37 (2001).
74. J.-J. Wu and C.-C. Yu, "Aligned TiO_2 Nanorods and Nanowalls," *J. Phys. Chem. B,* **108** [11] 3377-79 (2004).
75. J.-M. Wu, H. C. Shih, and W.-T. Wu, "Electron Field Emission from Single Crystalline TiO_2 Nanowires Prepared by Thermal Evaporation," *Chem. Phys. Lett.,* **413** [4-6] 490-94 (2005).
76. J.-M. Wu, H. C. Shih, W.-T. Wu, Y.-K. Tseng, and I.-C. Chen, "Thermal Evaporation Growth and the Luminescence Property of TiO_2 Nanowires," *J. Cryst. Growth,* **281** [2-4] 384-90 (2005).
77. B. Xiang, Y. Zhang, Z. Wang, X. Luo, Y. Zhu, H. Zhang, and D. Yu, "Field-Emission Properties of TiO_2 Nanowire Arrays," *J. Phys. D: Appl. Phys.,* **38** [8] 1152 (2005).
78. M. Ayers and A. Hunt, "Titanium Oxide Aerogels Prepared from Titanium Metal and Hydrogen Peroxide," *Mater. Lett.,* **34** [3-6] 290-93 (1998).
79. L. Campbell, B. Na, and E. Ko, "Synthesis and Characterization of Titania Aerogels," *Chem. Mater.,* **4** [6] 1329-33 (1992).
80. S.-S. Hong, M. S. Lee, S. S. Park, and G.-D. Lee, "Synthesis of Nanosized TiO_2/SiO_2 Particles in the Microemulsion and their Photocatalytic Activity on the Decomposition of p-Nitrophenol," *Catal. Today,* **87** [1-4] 99-105 (2003).
81. K. D. Kim, S. H. Kim, and H. T. Kim, "Applying the Taguchi Method to the Optimization for the Synthesis of TiO_2 Nanoparticles by Hydrolysis of TEOT in Micelles," *Colloids Surf., A,* **254** [1-3] 99-105 (2005).
82. A. Ali and W.-C. Oh, "Preparation of Ag_2Se-Graphene-TiO_2 Nanocomposite and its Photocatalytic Degradation (Rh B)," *J. Korean Ceram. Soc.,* **54** [5] 388-94 (2017).
83. Z. Li, H. Yang, F. Wu, J. Fu, L. Wang, and W. Yang, "Single-Crystalline Self-Branched Anatase Titania Nanowires for Dye-Sensitized Solar Cells," *Electron. Mater. Lett.,* **13** [2] 174-78 (2017).
84. Y. Lin, G. Wu, X. Yuan, T. Xie, and L. Zhang, "Fabrication and Optical Properties of TiO_2 Nanowire Arrays Made by Sol-Gel Electrophoresis Deposition into Anodic Alumina Membranes," *J. Phys.: Condens. Matter.,* **15** [17] 2917-22 (2003).
85. S. Lee, C. Jeon, and Y. Park, "Fabrication of TiO_2 Tubules by Template Synthesis and Hydrolysis with Water Vapor," *Chem. Mater.,* **16** [22] 4292-95 (2004).
86. S. Liu, L. Gan, L. Liu, W. Zhang, and H. Zeng, "Synthesis of Single-Crystalline TiO_2 Nanotubes," *Chem. Mater.,* **14** [3] 1391-97 (2002).
87. J. Qiu, W. Yu, X. Gao, and X. Li, "Sol-Gel Assisted ZnO Nanorod Array Template to Synthesize TiO_2 Nanotube Arrays," *Nanotechnology,* **17** [18] 4695 (2006).
88. D. M. Andoshe, S. Choi, Y.-S. Shim, S. H. Lee, Y. Kim, C. W. Moon, D. H. Kim, S. Y. Lee, T. Kim, and H. K. Park, "A Wafer-Scale Antireflective Protection Layer of Solution-Processed TiO_2 Nanorods for High Performance Silicon-Based Water Splitting Photocathodes," *J. Mater. Chem. A,* **4** [24] 9477-85 (2016).
89. Y. Chung, W. Lo, and G. Somorjai, "Low Energy Electron Diffraction and Electron Spectroscopy Studies of the Clean (110) and (100) Titanium Dioxide (Rutile) Crystal Surfaces," *Surf. Sci.,* **64** [2] 588-602 (1977).
90. M. Ramamoorthy, D. Vanderbilt, and R. King-Smith, "First-Principles Calculations of the Energetics of Stoichiometric TiO_2 Surfaces," *Phys. Rev. B,* **49** [23] 16721 (1994).
91. A. Barnard and L. Curtiss, "Prediction of TiO_2 Nanoparticle Phase and Shape Transitions Controlled by Surface Chemistry," *Nano Lett.,* **5** [7] 1261-66 (2005).
92. I. S. Cho, Z. Chen, A. J. Forman, D. R. Kim, P. M. Rao, T. F. Jaramillo, and X. Zheng, "Branched TiO_2 Nanorods for Photoelectrochemical Hydrogen Production," *Nano Lett.,* **11** [11] 4978-84 (2011).
93. F. Su, T. Wang, R. Lv, J. Zhang, P. Zhang, J. Lu, and J. Gong, "Dendritic Au/TiO_2 Nanorod Arrays for Visible-Light Driven Photoelectrochemical Water splitting," *Nanoscale,* **5** [19] 9001-9 (2013).
94. H. Qi, J. Wolfe, D. Fichou, and Z. Chen, "Cu_2O Photocathode for Low Bias Photoelectrochemical Water Splitting Enabled by NiFe-Layered Double Hydroxide Co-Catalyst," *Sci. Rep.,* **6** 30882 (2016).
95. Y. Yang, D. Xu, Q. Wu, and P. Diao, "Cu_2O/CuO Bilayered

Composite as a High-Efficiency Photocathode for Photoelectrochemical Hydrogen Evolution Reaction," *Sci. Rep.,* **6** 35158 (2016).
96. H. Gerischer, "On the Stability of Semiconductor Electrodes against Photodecomposition," *J. Electroanal. Chem. Interfacial Electrochem.,* **82** [1-2] 133-43 (1977).
97. A. Paracchino, V. Laporte, K. Sivula, M. Grätzel, E. Thimsen, "Highly Active Oxide Photocathode for Photoelectrochemical Water Reduction," *Nat. Mater.,* **10** [6] 456 (2011).
98. S. Emin, F. Abdi, M. Fanetti, W. Peng, W. Smith, K. Sivula, B. Dam, and M. Valant, "A Novel Approach for the Preparation of Textured CuO Thin Films from Electrodeposited CuCl and CuBr," *J. Electroanal. Chem.,* **717** 243-49 (2014).
99. C.-Y. Chiang, Y. Shin, K. Aroh, and S. Ehrman, "Copper Oxide Photocathodes Prepared by a Solution Based Process," *Int. J. Hydrogen Energy,* **37** [10] 8232-39 (2012).
100. A. C. Cardiel, K. J. McDonald, and K.-S. Choi, "Electrochemical Growth of Copper Hydroxy Double Salt Films and Their Conversion to Nanostructured p-Type CuO Photocathodes," *Langmuir,* **33** [37] 9262-70 (2017).
101. C. G. Read, Y. Park, and K.-S. Choi, "Electrochemical Synthesis of p-type $CuFeO_2$ Electrodes for Use in a Photoelectrochemical Cell," *J. Phys. Chem. Lett.,* **3** [14] 1872-76 (2012).
102. N. T. Hahn, V. C. Holmberg, B. A. Korgel, and C. B. Mullins, "Electrochemical Synthesis and Characterization of p-$CuBi_2O_4$ Thin Film Photocathodes," *J. Phys. Chem. C,* **116** [10] 6459-66 (2012).
103. G. P. Wheeler and K.-S. Choi, "Photoelectrochemical Properties and Stability of Nanoporous p-Type $LaFeO_3$ Photoelectrodes Prepared by Electrodeposition," *ACS Energy Lett.,* **2** [10] 2378-82 (2017).
104. J. Y. Kim, G. Magesh, D. H. Youn, J. W. Jang, J. Kubota, K. Domen, and J. S. Lee, "Single-Crystalline, Wormlike Hematite Photoanodes for Efficient Solar Water Splitting," *Sci. Rep.,* **3** 2681 (2013).
105. W. Cheng, J. He, Z. Sun, Y. Peng, T. Yao, Q. Liu, Y. Jiang, F. Hu, Z. Xie, B. He, and S. Wei, "Ni-Doped Overlayer Hematite Nanotube: A Highly Photoactive Architecture for Utilization of Visible Light," *J. Phys. Chem. C,* **116** [45] 24060-67 (2012).
106. J. M. Jeon, T. L. Kim, Y. S. Shim, Y. R. Choi, S. Lee, K. C. Kwon, S. H. Hong, Y. W. Kim, S. Y. Kim, M. Kim, and H. W. Jang, "Microscopic Evidence for Strong Interaction between Pd and Graphene Oxide that Results in Metal-Decoration-Induced Reduction of Graphene Oxide," *Adv. Mater.*, **29** [45] 1605929 (2017).